

Universitat Politècnica de Catalunya
Departament d'Enginyeria Electrònica

**Control of Grid-Connected Three-Phase Three-Wire
Voltage-Sourced Inverters Under Voltage Disturbances**

Doctoral Thesis

Submitted as a Compendium of Publications

Miguel Andrés Garnica López

Director: Dr. José Luis García de Vicuña Muñoz de la Nava

Co-director: Dr. Jaume Miret i Tomàs

November 2018

*Dedicado a mi amada familia, a mis
padres y hermanos, mi razón de ser.*

Abstract

The present doctoral thesis, submitted as a compendium of publications, focuses on designing control schemes for three-phase three-wire voltage-sourced inverters connected to the grid under voltage disturbances. The research recognizes the large-scale integration of distributed power generation systems into the network and takes advantage of this circumstance to investigate and develop new control strategies in order to provide better support to the modern power grid.

As a first contribution, a new algorithm to maximize power delivery capability of the inverter has been developed and experimentally tested under voltage imbalance conditions, i.e., during slight/shallow and deep asymmetrical sags. The algorithm of this control strategy meets grid code requirements, performs active power control, limits the maximum current injected by the inverter, and eliminates active power oscillations. As a result, six different cases of current injection were identified in this work, considering restrictions imposed by grid codes as well as different active-power production scenarios.

The second contribution of this research work has provided an experimental analysis of a low-voltage ride-through strategy whose voltage support capability had not been tested when voltage sags occur. This study was performed considering a scenario of multiple grid-connected inverters, different profiles of active power injection, and the equivalent grid impedance seen from the output side of each converter.

In the third contribution has been proposed a closed-loop controller for low-power distributed inverters that maximizes the current injection when voltage sag occurs. The control algorithm has been designed to meet grid code requirements and avoid overvoltage in non-faulty phases during grid faults. The controller is responsible for meeting coordinately several objectives and addressing the interactions that appear among them.

In the last two chapters, the argument of this doctoral thesis is complemented, the obtained experimental results are globally analyzed, finally, the present research work is concluded.

Resumen

Esta tesis doctoral, presentada en la modalidad de compendio de publicaciones en cumplimiento parcial de los requisitos para optar al título de Doctor en Ingeniería Electrónica de la Universidad Politécnica de Cataluña, se centra en el diseño de esquemas de control para inversores trifásicos conectados a la red eléctrica durante perturbaciones de voltaje. La investigación reconoce la integración a gran escala de los sistemas de generación distribuida en la red y aprovecha esta circunstancia para estudiar y desarrollar nuevas estrategias de control con el propósito de brindar un mejor soporte a la red eléctrica moderna.

Como primera contribución, se desarrolló un nuevo algoritmo para maximizar la capacidad de suministro de potencia del inversor en condiciones de desequilibrio de voltaje, es decir, durante caídas asimétricas de tensión leves, poco profundas y severas. El algoritmo de esta estrategia de control fue diseñado para cumplir los requerimientos de los vigentes códigos de red (*grid codes*), realizar control de la potencia activa, limitar la corriente máxima inyectada por el inversor y eliminar las oscilaciones de la potencia activa instantánea. Como resultado, en esta investigación se identificaron y validaron experimentalmente seis casos diferentes de inyección de corriente en la red, trabajo que tuvo en cuenta no solo las restricciones impuestas por los códigos de red, sino también los diferentes escenarios de producción de potencia activa.

La segunda contribución de este trabajo de investigación ha proporcionado el análisis experimental de una estrategia de inyección de corriente cuya capacidad de soporte de voltaje no se había probado durante fallos de red. Este estudio se realizó sobre un escenario de múltiples inversores conectados a la red eléctrica, utilizando diferentes perfiles de inyección de potencia activa y considerando, como aspecto fundamental para el análisis experimental, la impedancia de red equivalente vista desde el lado de salida de cada convertidor.

En la tercera contribución se diseñó un controlador en lazo cerrado para inversores distribuidos de baja potencia que maximiza la inyección de corriente cuando se produce una caída de tensión. Este algoritmo de control también satisface los requerimientos de los actuales códigos de red en cuanto a inyección de corriente reactiva durante fallos de red, pero cuenta con la capacidad adicional de evitar sobretensiones en las fases no defectuosas. De igual forma, este controlador es responsable de acometer coordinadamente varios objetivos y gestionar las interacciones que aparecen entre ellos.

En los últimos dos capítulos se complementa la unidad temática de esta tesis doctoral, se analizan globalmente los resultados experimentales obtenidos y, finalmente, se concluye el presente trabajo de investigación agregando, también, futuros campos de estudio.

Acknowledgment

For the achievements and all the support received during the development of his Doctoral Program in Electronic Engineering, the author wishes to express his gratitude in the first-person singular:

“I want to express my infinite gratitude to God for being my guide and putting in my way the right people to undertake this great challenge, to my beloved wife and my children for being my vital support, and to the Colombian Navy and COLFUTURO for the help and support provided in all moment.

When I speak of the right people to face this wonderful experience, I refer to my thesis directors, Dr. José Luis García de Vicuña Muñoz de la Nava and Dr. Jaume Miret i Tomàs. Their knowledge, research expertise, technical skills, and creative thinking have been vital for achieving the proposed objectives and always marked an appropriate course to reach safe harbor. My eternal gratitude for your support, guidance, and encouragement throughout my doctoral studies.

I also wish to express my sincere gratitude to the professors and researchers of the research group, Dr. Miguel Castilla Fernández, Dr. Antonio Camacho Santiago, and Dr. Ramón Guzmán Solà. Their great human qualities, example, and passion for research always fed my motivation and confidence to move forward with total determination. My warm thanks to Jordi Prat Tacias for welcoming my family from the first moment and for giving us their friendship and affection.

I also thank all my friends and laboratory colleagues who have been part of the research group. Thank you very much for your friendship and good advice Juan Rey, Carlos Alfaro, Javier Morales, Javier Torres, Lorena Sosa, Vangelis Papaioannou, Arash Momeneh, and Mohammad Moradi Ghahderijani.”

Contents

Abstract	iii
Resumen	v
Acknowledgment	vii
Contents	ix
1. Introduction	1
1.1 Motivation of this work	2
1.2 Argument of this thesis	2
1.3 Research objectives	6
1.4 Context and background of the topic	6
1.5 Thesis outline	12
1.6 Publications	13
Publications	14
2. Publication I:	16
<i>Control Strategy for Grid-Connected Three-Phase Inverters During Voltage Sags to Meet Grid Codes and to Maximize Power Delivery Capability</i>	17
2.1 Introduction	17
2.2 Grid-connected inverters under voltage sags	18
2.3 Proposed control objectives and control algorithm	19
2.4 Experimental results	24
2.5 Conclusion	30
2.6 References	30
2.7 Biographies	31
3. Publication II:	33
<i>Voltage Support Experimental Analysis of a Low-Voltage Ride-Through Strategy Applied to Grid-Connected Distributed Inverters</i>	34
3.1 Introduction	34
3.2 Multiple grid-connected inverters under voltage sags	36
3.3 Problem statement	38
3.4 Experimental results	42
3.5 Conclusions	49
3.6 References	50
4. Publication III:	55
<i>PI-Based Controller for Low-Power Distributed Inverters to Maximize Reactive Current Injection While Avoiding Over Voltage During Voltage Sags</i>	56
4.1 Introduction	56
4.2 Grid-connected inverters under voltage sags	57
4.3 Formulation of control objectives and proposed control algorithm	58
4.4 Design guidelines for the control loops	61
4.5 Experimental results	62
4.6 Comparison to previous control schemes	64

4.7	Conclusions	64
4.8	References	65
5.	Analysis of the results	68
5.1	Introduction	69
5.2	Basic topology of a grid-connected three-phase three-wire inverter	69
5.3	Deduction of the reference currents	70
5.4	Voltage support concept	73
5.5	Active and reactive power oscillations	75
5.6	Analysis of the maximum injected current	76
5.7	Analysis of the control algorithms	79
5.8	Analysis of the voltage support capability	81
6.	Conclusions and future work	84
6.1	Conclusions of the thesis	85
6.2	Future work	86
	References	88

1

Introduction

In this Chapter, the motivation to study control of grid-connected three-phase three-wire voltage-sourced inverters when voltage disturbances occur is presented, and the objectives that justify the argument of this work are established. Finally, the background and structure of the thesis are addressed.

Summary

- 1.1 Motivation of this work
 - 1.2 Argument of this thesis
 - 1.3 Research objectives
 - 1.4 Context and background of the topic
 - 1.5 Thesis outline
 - 1.6 Publications
-

1.1 Motivation of this work

The present research work has been developed within the *Grup de Recerca de Sistemes Electrònics de Potència i Control* at the *Universitat Politècnica de Catalunya*. All the experimental results have been obtained at the *Laboratori d'Electrònica de Potència* of the research group at the *Escola Politècnica Superior d'Enginyeria de Vilanova i la Geltrú*. The contributions of this thesis are presented as a compendium of three publications [1]–[3].

This doctoral thesis focuses its efforts on designing control strategies for three-phase three-wire voltage-sourced inverters (VSI) connected to the grid, set in the power-controlled current source mode, with the primary aim of improving the behavior of the electrical system during voltage disturbances, particularly during voltage sags. Therefore, this work intends to take advantage of all capabilities of inverters and provide them with auxiliary control functions to ensure that these disturbances, which may appear at their outputs, are eliminated or significantly reduced. The adequate injection of active and reactive currents of both positive and negative sequences—limiting the maximum output current—will be the key to avoid a widespread disconnection of distributed generation (DG) power facilities and achieve the desired control objectives.

Based on the works previously released by the Power and Control Electronics Systems Research Group [4]–[13] and by other researchers, this thesis addresses three different issues, each of them with a specific purpose closely related to the control objectives. Consequently, aspects not discussed in state of the art concerning low-voltage ride-through (LVRT) and grid codes (GCs), voltage support, and voltage regulation during voltage sags constitute the primary motivation of this thesis. This perspective has focused the research and findings in this field. The contributions of this work help understand better the mechanisms that lead to improving the features of the power system and, at the same time, protecting inverters during grid failures.

1.2 Argument of this thesis

The overall aim of this dissertation is to improve the performance of the electric power system (EPS) when a voltage disturbance is detected at the output of a grid-connected inverter delivering active power. Once such perturbation is detected, the conceived control algorithms are launched, and the reference currents are calculated based on the proposed control objectives. In this respect, the body of research of this thesis consists of four main chapters, of which three correspond to the published journal articles and one to the global analysis of the obtained results.

1.2.1 Control strategy for grid-connected three-phase inverters during voltage sags to meet grid codes and to maximize power delivery capability

In the first contribution [1], the maximum current of the inverter is injected following GC requirements to avoid the disconnection of DG power facilities during voltage sags. This work allows understanding a problem already studied in the literature, but providing as a novelty a new multi-objective control algorithm that manages the requirements and restrictions of a GC. The proposed algorithm contemplates six methods of current injection according to different active-power production scenarios and several voltage sag profiles. This research work has as significant precedents in the literature, among others, the studies carried out in [5]–[7], [10], [11], [13], and [14]–[21].

From this perspective, control of injected currents to avoid disconnection of distributed generation sources (DGSs) due to overcurrent has been proposed in [5], [15], [17]–[19]. However, the harmonic distortion percentage increases in [5], the active power cannot be injected under unbalanced faults in [15], [17], the delivered power shows undesired oscillations in [18], and the controller reference currents may exceed the inverter current capability under severe failures in [19].

Reactive power injection to provide voltage support when balanced and unbalanced faults occur has been presented in [6], [7], [10]. The approach in [6] presents a positive- and negative-sequence reactive current injection (RCI) protocol that provides flexible voltage support without requiring closed-loop control; nevertheless, a basic strategy is selected to generate the references of active current, in which only positive-sequence voltage is considered. References [7], [10] propose controllers for high-power DGSs with the purpose of restoring faulted phase voltages within the boundaries of continuous operation, but active power delivery is completely suspended.

New algorithms considering certain specific techniques to maximize some power capabilities of the inverter are proposed in [11], [13], [20], [21]. The controller introduced in [11] provides different LVRT services, but its control algorithm is complex when compared with previous schemes; the algorithm implemented in [13] focuses on distributed photovoltaic (PV) systems and gives priority to active power delivery; the E.ON code is applied in [20], but the control strategy focuses on the maximum power point tracking (MPPT) of the boost converter for PV power systems; and two GCs are considered in [21], but the proposed method cannot avoid oscillations in the active power when only reactive current is injected into the grid.

Different controllers are compared in [14]. Even though all of them can meet LVRT requirements, all the proposed control objectives cannot be achieved at the same time. Finally, it can be seen that in [14]–[17], [19] each control strategy determines the degree of power quality delivered to the network.

Therefore, compared with the works previously described, the control strategy proposed as the first contribution of the thesis is relevant for any DGS since it gives priority to reactive power injection (as established by current GCs), performs active power control, limits the maximum current of the inverter, and avoids active power oscillations.

1.2.2 Voltage support experimental analysis of a low-voltage ride-through strategy applied to grid-connected distributed inverters

The second contribution [2] focuses on using a control algorithm validated only for current injection, but in a network environment in which several inverters interact, an aspect hardly discussed in the literature [22]–[29]. In this work, the research focusing on the study of voltage support capability of inverters connected to networks with inductive and resistive characteristics.

In a comprehensive literature review about scenarios of multiple inverters connected to the grid, many exciting works have been identified, but most of them only present simulation results [22]–[26], [29] and only a few studies provide experimental results [27], [28].

In this respect, the coordinated operation between a wind farm and a static synchronous compensator (STATCOM) in a power network is studied in [22]; a control scheme of allocation of reactive power to maximize resource sharing of grid-connected inverters is proposed in [23]; the contributions made in [24]–[26] are based on the study of a real PV low-voltage (LV) grid in Denmark, and these papers formulate the application of reactive power control as an optimization problem to mitigate the overvoltage issue existing in LV grids with high penetration of PV technologies; and a complete study of a grid-connected industrial microgrid with two PV generators is carried out in [29], where sophisticated but complex control schemes are compared.

On the other hand, about the works that provide experimental results, a control strategy of automatic mode transition for multiple inverters is proposed in [27], and a real laboratory setup composed of four nodes is introduced in [28]. In this last work three tests are conducted; in the first test, the four nodes are configured as network-feeding converters, that is, the converters are programmed as power controlled current sources, emulating four PV-generation modules.

Hence, the second contribution of this thesis has provided an experimental analysis of an LVRT strategy whose voltage support capability had not been tested when voltage sags occur. This study was performed considering a scenario of multiple grid-connected inverters, different profiles of active power injection, and the equivalent grid impedance seen from the output side of each converter.

This second work also motivated the search for control strategies that would allow the optimization of the voltage support in RL grids. The analysis of the literature showed that only a limited number of works [30]–[34] deal with the voltage support considering these networks, which contrasts with the interest of the subject since no network is purely inductive or purely resistive [35], [36]. Addressing the voltage support with a perspective of RL grids provides a much more realistic view of this subject.

1.2.3 PI-based controller for low-power distributed inverters to maximize reactive current injection while avoiding over voltage during voltage sags

The third contribution [3] introduces a novel controller for low-power distributed inverters that maximizes the current injection when voltage sag occurs. Several positive- and negative-sequence current-injection protocols have been proposed in the literature to overcome overcurrent and overvoltage problems in one or more phases. Some of these current-injection protocols have been previously cited, but it is worth adding [37]–[44].

By drawing on the concept of overcurrent, positive- and negative-sequence RCI protocols have been proposed in different studies [1], [5], [11], [13], [18], [21]. The contributions made in [1], [13], [21], [39], [40], [43], [44] also provide additional functionalities during unbalanced voltage sags, among which reduction of dc-link oscillations stands out.

The relationship between RCI and voltage support capability in mainly inductive grids has been widely investigated [6]–[8], [10], [12], [37], [38], [41]–[43]. In general, works such as those carried out in [7], [8], [10], [37], [38], [42] propose controllers based on the injection of positive and negative sequences to restore faulted phase voltages within their limits of continuous operation. Likewise, a scheme similar to that presented in [6] is implemented in [30] to study the effect of active power injection in resistive grids, and a proposal based on controlling amplitude and phase angle of negative-sequence current to minimize negative-sequence voltage is made in [43].

In the context of low-power DGSs, it is important to note that some works have addressed the problems of overcurrent and overvoltage separately, but that very few have tried to solve them simultaneously [12], [41]. However, these control methods have some drawbacks. In [12], the control operates in open loop, an accurate estimation of the grid impedance is required, and the complex mathematical calculation of the reference currents requires a complete active power curtailment. In [41], the injection of the allowable maximum reactive current is not an objective, and the method used to avoid overvoltage is to make the reactive current equal to zero in non-faulty phases, which also makes the voltage support equal to zero for slightly dropped phases.

In this respect, the third contribution of this thesis proposes a complete control scheme that overcomes the limitations of the previous works. The proposed control algorithm meets GC requirements (LVRT and RCI) while avoiding overvoltage in non-faulty phases during grid faults. Besides, a closed-loop controller is responsible for meeting coordinately several objectives and addressing the interactions that appear among them.

1.2.4 General analysis

The way in which the journal articles relate to each other and contribute to the central theme of the thesis is shown in Chapter 5. This chapter complements the argument of the present dissertation and unifies the analysis in terms of active and reactive currents injected into the grid. The final discussion tends towards optimal voltage support with

two main premises: 1) limiting inverter maximum current to its nominal value and 2) mitigating oscillations of instantaneous active power.

The problem has been covered from different perspectives and network conditions, always ensuring that VSI systems operate safely—without exceeding their output current limits—and seeking delivery of active power without oscillations whenever possible since, in a grid-connected inverter, oscillations in the instantaneous power due to grid unbalance conditions can cause variation of the dc-link voltage. The control of the DC voltage, one of the basic tasks of the grid-side controller (see Table 1.5) [45], passes through the control of the power exchanged by the inverter with the grid and can be done either by controlling the current or controlling the AC voltage across the capacitor [46].

In summary, three-phase inverters in DG systems can help overcome imbalances and voltage anomalies that arise in the electrical network in order to guarantee the stability and reliability of the modern power system.

1.3 Research objectives

In this doctoral thesis, three research objectives have been formulated considering the concepts previously presented as well as the challenges and trends identified on control of grid-connected inverters:

Objective 1. To design a new multi-objective control scheme for three-phase inverters connected to the grid under voltage sags with injection capability of active and reactive currents via positive and negative sequences.

Objective 2. To perform a voltage-support experimental analysis of an LVRT current injection strategy in a complex scenario of multiple inverters connected to RL networks during voltage sags.

Objective 3. To design a new closed-loop multi-objective control scheme for low-power distributed inverters connected to the grid under voltage sags with both active and reactive current injection and voltage regulation capabilities.

1.4 Context and background of the topic

This Section presents the background of the research work with the aim of providing a broad context to the information discussed throughout the doctoral thesis. Besides, it seeks to link the research objectives with the research topic through a logical flow of ideas and to help readers understand the reasons for conducting the present investigation.

1.4.1 Overview of power generation, transmission, and distribution system

Large power plants and their long transmission lines have been the main components of traditional electricity infrastructure. At the generation site, bulky conventional transformers step the voltage up to long-distance transmission-line levels. These voltage values can be reduced for regional distribution using sub-transmission lines. At the main consumption centers, transformers located in distribution-system substations step the voltage down, and feeder lines carry the power to the end customers [47], [48].

In contrast to the conventional power distribution system with unidirectional power flow, environmental problems of recent decades have promoted the use of clean energies throughout distributed generation systems (DGSs), which are characterized by bringing generation centers closer to the consumption ones [49]. This new scenario involves environmental and energy improvements since it stimulates the development of renewable energies and reduces costs and losses [50].

The current and complex multi-source system has active functions and bidirectional power flow capability. This new scenario allows the grid to guarantee not only load-management but also demand-management, as well as the use of electricity market prices and forecast of energy to optimize the distribution system entirely [49].

1.4.2 Distributed generation and connection to the network

Some of the main definitions that can be found in the literature on the current dispersed or distributed generation model are collected and compared in [51]. However, it could be said that DG is a small-scale generation and that its technologies have already reached a stage of development that allows their large-scale implementation into the existing power system [52].

Technology	Renewable	Nonrenewable
Solar, photovoltaic or thermal	x	
Wind	x	
Geothermal	x	
Ocean	x	
Internal combustion engine		x
Combined cycle		x
Combustion turbine		x
Microturbines		x
Fuel cell		x

It should be noted that DG can include synchronous and induction generators, internal combustion engines, gas microturbines, wind turbines, fuel cells, solar photovoltaics [53], etc. As can be seen from Table 1.1, these technologies can be categorized as renewable

and nonrenewable [54]. If some DG technologies were fully implemented, they could worsen current pollution problems. Renewable energy (RE) is obtained from virtually inexhaustible natural sources, either because of the immense amount of energy they contain or because they are capable of regenerating by natural means [55]. It comprises those methods of obtaining energy that can operate indefinitely without emitting greenhouse gases, essential not only for energy efficiency but also for decarbonization, as shown in Table 1.2 [56].

Table 1.2 Reducing carbon dioxide emissions – “decarbonization”	
1. Renewable energies (REs)	
	Hydropower generation
	Hydraulic turbines (rivers)
	Marine energy—wave power and tidal power (oceans)
	Solar energy
	Solar thermal power generation
	Solar photovoltaic (PV) electricity
	Wind power
	Wind turbines
	Geothermal power generation
	Heat pump (HP) systems
2. Nuclear generation	
3. CO ₂ (carbon) capture and storage (CCS)	

At present, many factors could lead to new types of agreements and changes in the electric power industry. Among the most important ones are the following: Increase in the number of renewable energy sources connected to the utility grid together with advances in energy storage and control systems, and potential government incentive programs. The above mentioned, as a whole, will surely attract the attention of other sectors that have not yet used electricity, and this influence would have a positive impact on the environment, reflected in an additional reduction of CO₂.

1.4.3 Grid codes

Although the large-scale integration of DGSs can negatively impact the stability and reliability of power system, mainly during grid faults, it also provides meaningful opportunities to develop new control strategies with multiple features to better support the modern network. Countries with a high penetration level of inverter-based distributed generators operating in grid-connected mode are defining, updating and redefining their network interconnection requirements [57]–[66]. These specifications indicate fault profiles that these systems must support and procedures they must follow [67]–[73].

In compliance with these requirements, DG power facilities must remain connected to the network according to a voltage against time curve at the connection point during voltage sags. This capability is known as low-voltage ride-through and can be provided by each inverter injecting active and reactive powers into the network according to a grid code to support the power system and reduce the risk of voltage collapse during grid faults. These specifications are being reflected in the most recent GCs to take full advantage of the benefits of modern electric power grids but under appropriate safety and reliability conditions.

1.4.4 Voltage disturbances

Power quality refers to a wide variety of electromagnetic phenomena that characterize the voltage and current signals at a given time and place on the power system [74]. The increasing use of electronic equipment that may cause electromagnetic disturbances or that may be sensitive to these phenomena has increased the interest in this subject during the last years [75]. Electromagnetic phenomena are classified by the IEC into several groups as shown in Table 1.3 [74].

Table 1.3 Principal phenomena causing electromagnetic disturbances as classified by the IEC [76]	
Group	Examples
Conducted low-frequency phenomena	Harmonics, interharmonics Signal systems (power line carrier) Voltage fluctuations Voltage sags and interruptions Voltage imbalance Power-frequency variations Induced low-frequency voltages DC in AC networks
Radiated low-frequency phenomena	Magnetic fields Electric fields
Conducted high-frequency phenomena	Induced continuous wave (CW) voltages/currents Unidirectional transients Oscillatory transients
Radiated high-frequency phenomena	Magnetic fields Electric fields Electromagnetic fields Continuous waves Transients
Electrostatic discharge phenomena (ESD)	
Nuclear electromagnetic pulse (NEMP)	

As indicated in the IEEE Std 1159™-2009 [74], short-duration voltage variations are practically caused by fault conditions, energization of large loads, or intermittent loose connections in power wiring. Depending on the fault location and the system conditions, the fault can cause temporary voltage rises, voltage sags, or a complete loss of voltage.

Categories	Typical spectral content	Typical duration	Typical voltage magnitude
Transients			
Impulsive			
Nanosecond	5 ns rise	< 50 ns	
Microsecond	1 μ s rise	50 ns – 1 ms	
Millisecond	0.1 ms rise	> 1 ms	
Oscillatory			
Low frequency	< 5 kHz	0.3–50 ms	0–4 p.u.
Medium frequency	5–500 kHz	20 μ s	0–8 p.u.
High frequency	0.5–5 MHz	5 μ s	0–4 p.u.
Short-duration rms variations			
Instantaneous			
Sag		0.5–30 cycles	0.1–0.9 p.u.
Swell		0.5–30 cycles	1.1–1.8 p.u.
Momentary			
Interruption		0.5 cycles – 3 s	< 0.1 p.u.
Sag		30 cycles – 3 s	0.1–0.9 p.u.
Swell		30 cycles – 3 s	1.1–1.4 p.u.
Temporary			
Interruption		> 3 s – 1 min	< 0.1 p.u.
Sag		> 3 s – 1 min	0.1–0.9 p.u.
Swell		> 3 s – 1 min	1.1–1.2 p.u.
Long-duration rms variations			
Interruption, sustained		> 1 min	0.0 p.u.
Undervoltages		> 1 min	0.8–0.9 p.u.
Overvoltages		> 1 min	1.1–1.2 p.u.
Current overload		> 1 min	
Imbalance			
Voltage		steady state	0.5–2%
Current		steady state	1.0–30%
Waveform distortion			
DC offset		steady state	0–0.1%
Harmonics	0–9 kHz	steady state	0–20%
Interharmonics	0–9 kHz	steady state	0–2%
Notching		steady state	
Noise	broadband	steady state	0–1%
Voltage fluctuations	< 25 Hz	intermittent	0.1–7%
Power frequency variations		< 10 s	\pm 0.10 Hz

The impact on the voltage during the fault condition, which can be close to or remote from the point of interest, is a short duration variation.

Voltage sags are the main power quality concern for process industries as well as for most utilities and their customers [77], [78]. From [79], [80], it can be said that a voltage sag is a temporary reduction of the root-mean-square (rms) voltage at a point in the electrical system below a threshold. Voltage sags are generally caused by faults that typically occur within the customer facility or on the utility transmission and distribution systems. Starting large loads can also cause voltage sags that last several seconds. However, fault-induced sags are much more severe than sags due to the starting of large loads. Equipment

failure, lightning, tree limbs, and animal contact have been identified as the primary reasons for fault-induced voltage sags [78].

Table 1.4, extracted from the IEEE Std 1159™-2009 [74], provides additional information regarding typical spectral content, duration, and magnitude for each category of electromagnetic phenomena used for power quality community. Table 1.4 allows seeing a big picture of the different electromagnetic phenomena to identify the place occupied by the voltage sags. All categories of the voltage sags have the same range of voltage magnitude [in per unit (p.u.)], a decrease in rms voltage to typical values between 0.1 p.u. and 0.9 p.u., but the typical duration of the sags is different in each category.

1.4.5 Inverters and static power converters

Power electronic (or static) converter is defined in [81] as a multiport circuit that is composed of electronic switches, and that can also include auxiliary components such as capacitors, inductors, and transformers. The primary function of a converter is to facilitate the exchange of energy between two or more subsystems based on pre-specified performance requirements.

The range of applications for power electronics converters is so extensive that it goes from low power residential and traditional applications to high power transmission lines, but emerging applications on RE systems have generated more significant interest [49].

As explained in the IEEE Std 1547.2™-2008 [82], distributed resources (DRs) or distributed energy resources offer a variety of possibilities for energy conversion and electric power generation. Several energy sources, fuels, and converters are used to provide electricity through different technologies mentioned in Table 1.1. Three types of electrical converters are considered in the IEEE 1547 series of standards: synchronous generators, asynchronous generators, and static or electronic inverters. Static inverters can be supplied by DC generation/storage sources or by an AC generation source and an AC/DC converter. Their fundamental role in DR applications is to convert DC or non-synchronous AC electricity from a prime mover energy source into a synchronous AC system of voltages that can be efficiently interconnected with electric power systems (EPSs).

The importance of the control in distributed power generation systems (DPGSs) is highlighted in [45], where the authors divide the control tasks into two parts, as can be seen in Table 1.5.

It is essential to review the grid parameters, among them maximum voltage harmonic levels, maximum voltage unbalance, maximum voltage amplitude variations, maximum frequency variations, and voltage sag profile are of interest for designing the control of PV inverters [83]. Requirements for wind turbines [84] include not only behavior during normal operation, such as control of frequency and voltage deviations, active power control, and reactive power control, but also during grid disturbances, such as voltage ride-through (VRT) and RCI.

Input-side controller		Grid-side controller	
Main property	To extract the maximum power from the input source.	Basic tasks	<ul style="list-style-type: none"> • Control of active power generated to the grid. • Control of reactive power transfer between the DPGS and the grid. • Control of dc-link voltage. • Ensure high quality of the injected power. • Grid synchronization.
Basic task	To protect the input-side converter.	Ancillary services	<ul style="list-style-type: none"> • Local voltage and frequency regulation. • Voltage harmonic compensation. • Active filtering.

1.5 Thesis outline

The present doctoral thesis has been organized following the contributions published in specialized journals in this field of knowledge. The sequence of chapters, after the Introduction, is as detailed below:

Chapter 1 deals with the Introduction of the present doctoral thesis.

Chapter 2 is devoted to a control strategy for grid-connected three-phase inverters during voltage sags, which meets GCs and maximizes power delivery capabilities.

Chapter 3 provides an experimental analysis of an LVRT strategy for multiple grid-connected inverters in order to help support the grid during voltage sags.

Chapter 4 is dedicated to a PI-based control strategy for low-power distributed inverters that meets GCs, maximizes reactive current injection, and avoids overvoltage during voltage sags.

Chapter 5 addresses the global discussion of the results obtained during the development of the thesis.

Chapter 6 concludes the doctoral thesis and raises new research expectations that the present work suggests.

1.6 Publications

The journal and congress articles published during the development of the doctoral thesis are mentioned in this Section. The first three journal articles (i)–(iii) make up the compendium of publications.

- (i). M. A. Garnica Lopez, J. L. Garcia de Vicuna, J. Miret, M. Castilla, and R. Guzman, “Control Strategy for Grid-Connected Three-Phase Inverters During Voltage Sags to Meet Grid Codes and to Maximize Power Delivery Capability,” *IEEE Trans. Power Electron.*, vol. 33, no. 11, pp. 9360–9374, Nov. 2018.
- (ii). M. Garnica, L. García de Vicuña, J. Miret, A. Camacho, and R. Guzmán, “Voltage Support Experimental Analysis of a Low-Voltage Ride-Through Strategy Applied to Grid-Connected Distributed Inverters,” *Energies*, vol. 11, no. 8, p. 1949, Jul. 2018.
- (iii). J. Miret, M. Garnica, M. Castilla, L. García de Vicuña, and A. Camacho, “PI-based controller for low-power distributed inverters to maximize reactive current injection while avoiding over voltage during voltage sags,” *IET Power Electron.*, *in press*.
- (iv). M. A. Garnica López, L. García de Vicuña, J. Miret, P. Marti, and M. Velasco, “Control strategy to maximize the power capability of PV-based industrial microgrids during voltage sags,” in *IECON 2017 - 43rd Annual Conference of the IEEE Industrial Electronics Society*, 2017, pp. 1001–1006.
- (v). M. Moradi Ghahderijani, M. Castilla, J. M. Rey, J. Martínez Torres, and M. A. Garnica López, “A communication-less control scheme for a variable air-gap wireless energy transfer system using current source resonant converter,” in *IECON 2017 - 43rd Annual Conference of the IEEE Industrial Electronics Society*, 2017, pp. 509–514.
- (vi). A. Camacho, M. Castilla, J. Miret, L. García de Vicuña, and M. A. Garnica López, “Control Strategy for Distribution Generation Inverters to Maximize the Voltage Support in the Lowest Phase During Voltage Sags,” *IEEE Trans. Ind. Electron.*, vol. 65, no. 3, pp. 2346–2355, Mar. 2018.

Publications

2

Publication I:

CONTROL STRATEGY FOR GRID-CONNECTED THREE-PHASE INVERTERS DURING VOLTAGE SAGS TO MEET GRID CODES AND TO MAXIMIZE POWER DELIVERY CAPABILITY

M. A. Garnica Lopez, J. L. Garcia de Vicuna, J. Miret, M. Castilla, and R. Guzman, "Control Strategy for Grid-Connected Three-Phase Inverters During Voltage Sags to Meet Grid Codes and to Maximize Power Delivery Capability," *IEEE Trans. Power Electron.*, vol. 33, no. 11, pp. 9360–9374, Nov. 2018.

ATTENTION;

You can consult the quoted article, included on pages 17 to 32 on the thesis, on the publisher's website <https://ieeexplore.ieee.org/document/8255642>

Summary

- 2.1 Introduction
 - 2.2 Grid-connected inverters under voltage sags
 - 2.3 Proposed control objectives and control algorithm
 - 2.4 Experimental results
 - 2.5 Conclusion
 - 2.6 References
 - 2.7 Biographies
-

3

Publication II:

VOLTAGE SUPPORT EXPERIMENTAL ANALYSIS OF A LOW-VOLTAGE RIDE-THROUGH STRATEGY APPLIED TO GRID-CONNECTED DISTRIBUTED INVERTERS





M. Garnica, L. García de Vicuña, J. Miret, A. Camacho, and R. Guzmán, “Voltage Support Experimental Analysis of a Low-Voltage Ride-Through Strategy Applied to Grid-Connected Distributed Inverters,” *Energies*, vol. 11, no. 8, p. 1949, Jul. 2018.

Summary

- 3.1 Introduction
 - 3.2 Multiple grid-connected inverters under voltage sags
 - 3.3 Problem statement
 - 3.4 Experimental results
 - 3.5 Conclusions
 - 3.6 References
-

Article

Voltage Support Experimental Analysis of a Low-Voltage Ride-Through Strategy Applied to Grid-Connected Distributed Inverters

Miguel Garnica ^{1,*} , Luís García de Vicuña ¹, Jaume Miret ¹ , Antonio Camacho ¹  and Ramón Guzmán ² 

¹ Department of Electronic Engineering, Technical University of Catalonia, 08800 Vilanova i la Geltrú, Spain; vicuna@eel.upc.edu (L.G.d.V.); jmiret@eel.upc.edu (J.M.); antonio.camacho.santiago@upc.edu (A.C.)

² Department of Automatic Control, Technical University of Catalonia, 08800 Vilanova i la Geltrú, Spain; ramon.guzman@upc.edu

* Correspondence: miguel.andres.garnica@upc.edu; Tel.: +34-93-896-7735

Received: 3 April 2018; Accepted: 24 July 2018; Published: 27 July 2018



Abstract: In recent decades, different control strategies have been designed for the increasing integration of distributed generation systems. These systems, most of them based on renewable energies, use electronic converters to exchange power with the grid. Capabilities such as low-voltage ride-through and reactive current injection have been experimentally explored and reported in many research papers with a single inverter; however, these capabilities have not been examined in depth in a scenario with multiple inverters connected to the grid. Only few simulation works that include certain methods of reactive power control to solve overvoltage issues in low voltage grids can be found in the literature. Therefore, the overall objective of the work presented in this paper is to provide an experimental analysis of a low-voltage ride-through strategy applied to distributed power generation systems to help support the grid during voltage sags. The amount of reactive power will depend on the capability of each inverter and the amount of generated active power. The obtained experimental results demonstrate that, depending on the configuration of distributed generation, diverse inverters could have different control strategies. In the same way, the discussion of these results shows that the present object of study is of great interest for future research.

Keywords: active and reactive current injection; distributed generation; low-voltage ride-through; multiple inverters; voltage sags; voltage support

1. Introduction

It is well known that electric power is fundamental for sustainable development because it is necessary for economic growth and because this same necessity stimulates new alternatives concerning renewable and clean energies [1]. The world's leading countries in the development of less polluting energy solutions are favoring the growth and expansion of distributed power generation systems (DPGSs) based on renewable sources [2]. Therefore, considering the wide-scale penetration of these systems in the distributed grid, power system operators have focused their attention on the challenge of maintaining reliability and stability of the electrical network by implementing and updating rigorous grid codes (GCs). These GCs are intended to limit the disconnection of these DPGSs under grid faults as much as possible and avoid loss of power generation that could yield to power outages [3–6].

Grid fault conditions can generate short-duration voltage variations—a decrease in rms voltages, typically between 0.1 p.u. and 0.9 p.u., for a period of 0.5 cycles to 1 min—one of the primary power quality concern for process industries [7,8]. Consequently, during grid faults, GCs demand that the distributed generation (DG) systems remain connected to the grid, support the voltage recovery,

and resume the active power feed-in after the fault clearance [9–11]. As a result of the increasing renewable power penetration level and the considerations mentioned above, latest GCs and power grid operators require low-voltage ride-through (LVRT) capability. This requirement means that DPGSs above a specific power range should stay connected during grid faults according to the corresponding time–voltage curve. This function shows the voltage disturbance area at the grid connection point that must be withstood by the facility. A capability that must not only be verified, but also certificated [12,13].

During the last years, numerous studies and investigations on different fault ride-through (FRT) control strategies for grid-connected inverters have been published in the literature, all intended to improve the behavior of the inverter during grid faults [14–27]. However, most of these strategies were presented for a single inverter connected to the grid. Nevertheless, some works address the issue of the operation of multiple inverter-based renewable distributed generators [28–34]. In the literature [28], the coordinated operation between a wind farm and a static synchronous compensator (STATCOM) in a power network is studied. This work also refers to an improved system that could use the inverter capability of a solar farm as a STATCOM device at night. However, despite making a good approximation and presenting an interesting proposal, the solution is not widely developed and no experimental results are presented. A control scheme of allocation of reactive power to maximize resource sharing of grid-connected inverters is proposed in the literature [29]. The studied power network considers several grid-connected inverters, but its topology includes both a point of common coupling (PCC) connected to the utility grid or a co-gen plant generator and a communication scheme that makes this control scheme appropriate for smart grids and microgrids. This work also presents only simulation results.

The contributions made in the works of [30–32] are based on the study of a real photovoltaic (PV) low-voltage (LV) grid located in Brædstrup, a village in the region of Østjylland, Denmark [35]. These papers formulate the application of reactive power control as an optimization problem to mitigate the overvoltage problem existing in LV grids with high penetration of PV technologies. In [31] a comparative analysis of five reactive power compensation techniques in these networks has also been presented. These works consider communication schemes and present simulation results.

In the literature [33], a control strategy of automatic mode transition for multiple inverters is proposed. When the grid is available, the inverters operate in current-control mode by injecting power into the network. When a grid failure occurs, all inverters automatically switch to the drop-control mode to achieve proportional power sharing and return to the current-control mode when network availability is restored. Nevertheless, the system under consideration—with a typical microgrid configuration—consists of two single-phase inverters, local loads, a bidirectional static transfer switch, and a synchronization switch. A hardware and software description of a real laboratory setup composed of four nodes is done in the literature [34]. This experimental network can emulate the two main scenarios of a dispersed generation network: (1) distributed generation sources connected to the grid and (2) microgrids in islanded mode. However, only in the first of the three tests, the four nodes work as network-feeding converters without additional comparisons with other profiles of generated power. Finally, a complete work of comparing sophisticated but complex control schemes is carried out in the literature [36]; nonetheless, the study for a grid-connected industrial microgrid with two PV generators is only validated with MATLAB simulations.

Considering this topic not only attractive but also absent in the literature, as far as authors' knowledge refers, this paper intends to make a first experimental approach to the injection of power by several DG systems connected to the grid (multiple inverters) when voltage sags occur. Consequently, a specific experimental platform with different combinations of impedance is used to analyze how a conventional current generator acts. This analysis will highlight the advantages and disadvantages of these injection procedures. Unlike the work of [37], the inverters do not make up a microgrid in this study.

The research objectives of this study, which are different from the control objectives of the strategies that can be implemented in the controllers, are grouped or summarized basically into two primary goals:

- To extend, in a scenario of multiple grid-connected inverters, the use or application of LVRT control strategy [25], whose voltage support capability has not been tested when voltage sags occur.
- To carry out an analysis of the experimental results of the power injection profiles (PIPs) as a function of the generated power (P_G) and the equivalent impedance seen from the output side of each converter.

This paper has been structured as follows. Section 2 describes the operation of multiple grid-connected inverters under voltage sags. The problem statement is presented in Section 3. The experimental results and a concise discussion on the behavior of the studied parameters are shown in Section 4. Finally, Section 5 presents the conclusions of the paper and briefly describes the research guidelines for future works.

2. Multiple Grid-Connected Inverters under Voltage Sags

This section deals with the description and characterization of the experimental distributed generation network connected to the grid under voltage sags. Also, the primary GC requirements during these disturbances are described.

2.1. Experimental Network Configuration

Figure 1 shows the implemented experimental network. A three-phase distributed generation network composed of four voltage-sourced inverters (VSIs) and one programmable AC power source, which emulates the utility grid, has been implemented in the power network laboratory (PNL). Details on the design and implementation of the experimental test bench can be found in the literature [34]. Each generation node (DPGS) is composed of a three-phase inverter with an output LC filter connected to the network through a wye-delta transformer. A DC power source feeds each inverter. The value of P_G is one of the inputs of each controller that will help determine the amount of injected power. The control block is responsible for driving the inverter switches to deliver power into the grid, giving priority to the active power according to the control algorithm of the strategy under test, but also to inject reactive power when necessary. The local voltages (v_1 to v_4) and the inverter currents (i_1 to i_4) are measured instantaneously to accomplish this task.

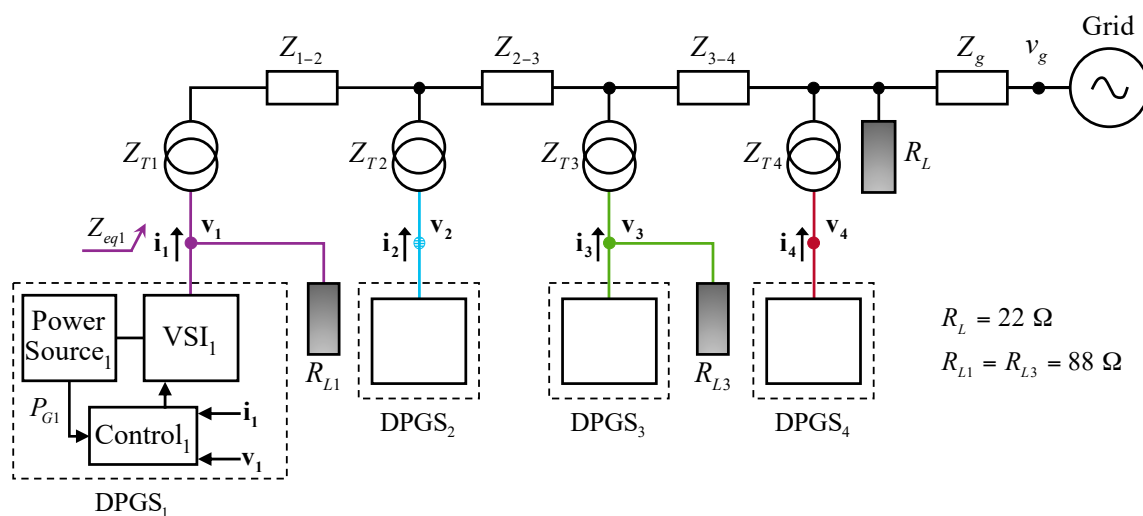


Figure 1. Scheme of the implemented experimental network. VSI—voltage-sourced inverter; DPGS—distributed power generation system; P_G —generated power.

The blocks Z_{1-2} , Z_{2-3} , and Z_{3-4} model the impedances of the lines connecting the distributed/dispersed nodes and the grid. The wye-delta transformer introduces the equivalent LCL output inductance L_T , as well as some parasitic resistance (see Table 1). The equivalent impedance of the transformer is used in the testbed to emulate lines with non-negligible resistive components.

Table 1. Line impedances.

Quantity	Acronym	Value
transformer equivalent inductances 1 and 2	$L_{T1,2}$	1.0 mH
transformer equivalent resistances 1 and 2	$R_{T1,2}$	0.5 Ω
transformer equivalent inductances 3 and 4	$L_{T3,4}$	0.6 mH
transformer equivalent resistances 3 and 4	$R_{T3,4}$	1.13 Ω
line inductance between 1 and 2	L_{1-2}	2.0 mH
line inductance between 2 and 3	L_{2-3}	0.8 mH
line inductance between 3 and 4	L_{3-4}	0.8 mH

As the equivalent impedance seen by each VSI is of particular interest, these data are shown in Table 2.

Table 2. Equivalent impedance seen from the output of the voltage-sourced inverters (VSIs). DPGS—distributed power generation system.

DPGS	R_{eq} (Ω)	L_{eq} (mH)	Z_{eq} (Ω)	Angle θ_{eq} (deg.)	$ Z_{eq} $ (Ω)
1	0.50	4.60	$0.50 + 1.73j$	73.92°	1.80
2	0.50	2.60	$0.50 + 0.98j$	62.97°	1.10
3	1.13	1.40	$1.13 + 0.53j$	25.04°	1.25
4	1.13	0.60	$1.13 + 0.23j$	11.32°	1.15

The equivalent impedance seen from the output side of each generator has been calculated by appropriately adding the impedance of lines, transformers, and loads.

2.2. Voltage Sag Characterization

The interaction between the power inverter and the network under balanced and unbalanced faults is a critical issue. However, the normal operation of the grid-connected inverters can be severely affected when unbalanced grid failures occur, because these faults generate negative-sequence voltages in the network [38,39]. The study of these voltage disturbances shows that the occurrence percentage of balanced faults (symmetrical three-phase faults) is very low, close to 3–2% [40].

The method of symmetrical components permits to extend the per phase analysis to systems with unbalanced loads or faults and provides a practical tool for understanding the operation of a three-phase system during unbalanced conditions [41–47]. However, as stated in the work of [39], “the interaction of the symmetrical components produces active and reactive power oscillations (\tilde{p} and \tilde{q}) at the output of the converter, which should be carefully controlled”.

During voltage sags, the instantaneous phase voltages (v_1 to v_4) at the output of each node (DPGS) can be described as the sum of their positive- and negative-symmetric sequences [38]. Applying Clarke’s transformation, these local voltages are expressed in the stationary reference frame (SRF) as

$$v_\alpha = v_\alpha^+ + v_\alpha^- = V^+ \cos(\omega t + \phi^+) + V^- \cos(\omega t + \phi^-) \quad (1)$$

$$v_\beta = v_\beta^+ + v_\beta^- = V^+ \sin(\omega t + \phi^+) - V^- \sin(\omega t + \phi^-) \quad (2)$$

where v_α and v_β are the instantaneous voltages expressed in the SRF, v_α^+ and v_β^+ are the positive-sequence voltages, v_α^- and v_β^- are the negative ones, and ω is the grid angular frequency. V^+ and V^- are the amplitudes of the positive- and negative-sequence voltages, respectively,

$$V^+ = \sqrt{(v_\alpha^+)^2 + (v_\beta^+)^2} \quad (3)$$

$$V^- = \sqrt{(v_\alpha^-)^2 + (v_\beta^-)^2} \quad (4)$$

and ϕ is the angle between the positive and negative sequences.

$$\phi = \phi^+ - \phi^- = \cos^{-1} \left(\frac{(v_\alpha^+ v_\alpha^-) - (v_\beta^+ v_\beta^-)}{V^+ V^-} \right) \quad (5)$$

Therefore, any voltage sag can be characterized by Equations (3)–(5).

Similarly, with the values of the voltage sequence amplitudes (V^+ and V^-), the effective voltage (V_e) can be calculated as indicated in the IEEE Std 1459™-2010 [48]:

$$V_e = \sqrt{(V^+)^2 + (V^-)^2} \quad (6)$$

This collective value concept, introduced by Buchholz to represent the voltages and currents collectively in a multiphase system [49], will be used to compare the voltage support responses obtained in the experimental results.

2.3. Requirements under Voltage Sags

In the absence of grid failures, each DPGS delivers its P_G into the grid while maintaining amplitude control of the injected currents. During voltage disturbances, GCs require additional services to maintain the integrity of the grid and increase its reliability. As a rule, under grid disturbances, wind GCs primarily require LVRT and RCI capabilities. Other GCs also require both active and reactive power injection to simultaneously feed and support the grid [10,11]. GCs for PV systems only require active power injection, although reactive power injection is a mandatory capability in some countries [50].

3. Problem Statement

This section presents the description of the problem that includes the concept of voltage support, a comparative analysis of different control strategies for generating reference currents in grid-connected converters, the formulation of the problem, and a brief explanation of the chosen control scheme.

3.1. Voltage Support Concept

The experiments carried out in this study take into account the complex impedance [51] of the lines. This fact allows addressing the voltage support concept, whose primary objective is to regulate the phase voltages within the limits established in GCs for continuous operation [18]. In this work, these voltages are not regulated, but experimental data are obtained to analyze the changes in local voltages due to the injected currents. As a result of the voltage support capability of each DPGS, the amplitudes of the positive- and negative-sequence voltages for each node, V_i^+ and V_i^- (for $i = 1$ to 4), can be expressed as a function of the equivalent grid voltage, the equivalent grid impedance (Z_{eqi}), and the injected current amplitudes as [52]

$$V_i^+ = R_{eqi} I_{pi}^+ + \omega L_{eqi} I_{qi}^+ + \sqrt{(V_{gi}^+)^2 - (\omega L_{eqi} I_{pi}^+ - R_{eqi} I_{qi}^+)^2} \quad (7)$$

$$V_i^- = R_{eqi}I_{pi}^- - \omega L_{eqi}I_{qi}^- + \sqrt{\left(V_{gi}^-\right)^2 - \left(\omega L_{eqi}I_{pi}^- + R_{eqi}I_{qi}^-\right)^2} \tag{8}$$

where $I_{pi}^+, I_{pi}^-, I_{qi}^+$, and I_{qi}^- are the current amplitudes associated with the active and reactive powers and V_{gi}^+ and V_{gi}^- are the amplitudes of the positive- and negative-sequence voltages at the grid side, respectively. Notice that V_g is not available in a practical application. Indeed, V_g is never used in the control algorithm (see Figure 2). Each local voltage vector \mathbf{v}_i is sensed at the output of its corresponding inverter and, therefore, these are the voltages used in the control algorithm.

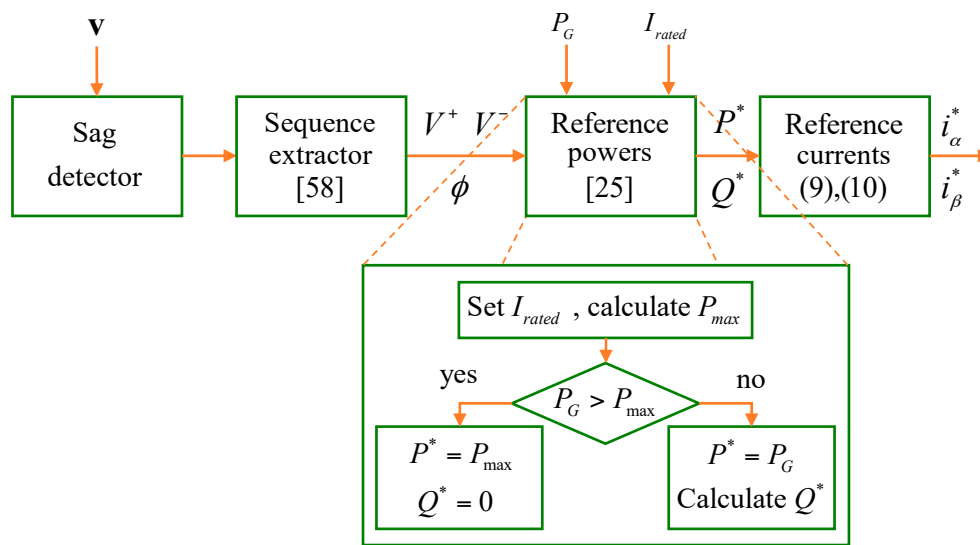


Figure 2. Block diagram of the control scheme.

In both Equations (7) and (8), the second term inside the radical is negligible; therefore, each square root becomes V_{gi}^+ and V_{gi}^- , respectively. As shown in Equation (7), the amplitudes of the positive-sequence currents (I_{pi}^+ and I_{qi}^+) increase the amplitude of the positive-sequence voltage (V_i^+). Now, it can be seen from Equation (8) that the product $R_{eqi} I_{pi}^-$ must be negative to reduce the amplitude of the negative-sequence voltage (V_i^-). From these two equations, it can be said that the voltage support solution is related to the different amplitudes of injected currents, but it is closely linked to the equivalent grid impedance.

When analyzing the voltage support effects, thanks to the use of symmetric sequences, the inverters can be viewed as current sources [53] that inject active and reactive currents into the grid via positive and negative sequences.

3.2. Comparison of the Principal Strategies for Generating Reference Currents in Grid-Connected Inverters

Different strategies and methods for generating the controller reference currents of a DG system—to deliver into the network active and reactive powers (P and Q), under unbalanced grid voltage conditions—can be found in the literature [19,39,54].

In this section, an injection method to implement a multi-inverter system with voltage support performances is chosen. The analysis that is carried out in this section compares different control strategies to identify their advantages and disadvantages. Active power oscillations, which can cause system malfunction; total harmonic distortion (THD), which can affect the energy quality generated by the inverter; and maximum current (I_{max}), which could be higher than the inverter rated current (I_{rated}) [19], are fundamental aspects to consider.

Based on the works of [54], the fundamental control strategies used to generate reference currents and their characteristics are summarized in Table 3, in which it is possible to see which have a better performance.

Table 3. Comparison of different strategies for generating reference currents. THD—total harmonic distortion; FBSS—flexible balance of symmetric sequences.

Strategy	Power Behavior	THD	I_{max}
IARC [39]	$\bar{p} \approx 0$ and $\bar{q} \approx 0$ negligible oscillations	high	high
AARC [39]	when $Q = 0 \Rightarrow \bar{p} \neq 0$ when $P = 0 \Rightarrow \bar{q} \neq 0$	low	low
BPSC [39,55]	$\bar{p} \neq 0$ and $\bar{q} \neq 0$ lower oscillations	low	low
ICPS [55]	if $Q \neq 0 \Rightarrow \bar{p} \neq 0$ if $P \neq 0 \Rightarrow \bar{q} \neq 0$	medium	high
PNSC [39,55]	when $P \neq 0$ and $Q = 0 \Rightarrow \bar{q} \neq 0$ when $P = 0$ and $Q \neq 0 \Rightarrow \bar{p} \neq 0$	low	high
ZSCC [56]	$\bar{p} = 0$ and $\bar{q} = 0$ four-wire or six-wire systems	low	very high
FPNSC [39]	$\bar{p} \neq 0$ and $\bar{q} \neq 0$ power oscillations	low	properly controllable
FBSS (L grids) [16,25]	$\bar{p} = 0$ and $\bar{q} \neq 0$ $\bar{q} = 0$ if $P = 0$ (special case)	low	properly controllable
FBSS (R grids) [57]	$P \neq 0$, $Q = 0$, and $\bar{q} \neq 0$ $\bar{p} = 0$ (special configuration)	low	properly controllable
VSS (RL grids) [52,53]	$\bar{p} \neq 0$ and $\bar{q} \neq 0$	low	properly controllable

It can be seen from the data in Table 3 that only few control strategies, IARC [39], ZSCC [56], and FBSS [16,25,57], avoid active power oscillations during voltage sags, which is especially important in PV applications. The set of reference currents used by the authors of [25] is based on the work of [16], a voltage support strategy that introduces the so-called “flexible balance of symmetric sequences (FBSS)”. Therefore, different control objectives will be achieved by tuning the control parameters to balance the positive- and negative-sequence voltages. One of those objectives is the cancellation of active power oscillations (\bar{p}), as these oscillations negatively affect the dc-link voltage and can provoke an inverter malfunction.

Regarding the reduction of the maximum current, BPSC [39,55], AARC [39], FPNSC [39], FBSS [16,25,57], and VSS [52,53] have the best performances, while ZSCC [56] is the least favorable. As for the harmonic distortion, the worst case is found in IARC [39], followed by ICPS [55]. The other strategies have low THD. In terms of the control complexity, it is also important to note that BPSC [39,55] and FBSS [16,25,57] are less complex than the others.

3.3. Problem Formulation

A certain impedance must be considered between the inverter connection point and the utility grid to test the voltage support capability. When providing voltage support to the grid during voltage sags, changes in the local voltage (v_i) due to the injected current (i_i) must be estimated. All the currents (i_1 to i_4) injected into the network will produce effects on the inverter output voltages (v_1 to v_4) due to the equivalent grid impedance Z_{eqi} [52].

Mainly, the control strategy [25] has been chosen to evaluate its effect on voltage support and because it has the following characteristics:

1. Capability to deliver both P and Q into the grid.
2. Current injection by positive and negative sequences (I_p^+ , I_q^+ , I_p^- and I_q^-).
3. Low THD.
4. Maximum current limitation.

5. Mitigation of active power oscillations.
6. Reduced complexity (control algorithm with a set of reduced instructions).

This control strategy has not been studied for voltage support and it was validated only for current injection considering a single inverter. As a contribution, the voltage support effects in the case of multi-inverter systems are analyzed in this work.

3.4. Control Scheme

The general procedure of this control strategy is depicted in Figure 2. Firstly, the voltage sag is detected. Secondly, the positive- and negative-voltage sequences (v_{α}^+ , v_{β}^+ and v_{α}^- , v_{β}^-) are obtained from the sequence extractor [58], and then the amplitudes (V^+ , V^-) are calculated by Equations (3) and (4). Afterwards, the power references (P^* , Q^*) are calculated based on the sag characteristics (V^+ , V^- and ϕ), the generated power (P_G), and the rated current (I_{rated}).

Note that the block of reference powers comprises the control algorithm. The maximum allowable active power (P_{max}) is always calculated and compared with P_G to protect the inverter. If P_G is higher than P_{max} , the controller applies an active power curtailment (APC) and sets $P^* = P_{max}$. During voltage sags, the control algorithm works in the same way and gives priority to the delivery of active power, but now each inverter is forced to inject I_{rated} because of the fault conditions. If P_G is less than P_{max} , then I_{rated} is not exceeded and, therefore, a determined amount of reactive power must be injected to reach I_{max} . Finally, the current references (i_{α}^* , i_{β}^*) are computed.

The objective of this strategy is to inject the rated current of the inverter and avoid oscillations of the active power when a voltage sag occurs. For this purpose, the control algorithm meets five conditions:

1. To prioritize injection of active power.
2. To inject the rated current.
3. To apply APC when $P_G > P_{max}$.
4. To inject reactive power into the grid when $P_G < P_{max}$ to reach I_{rated} .
5. To avoid active power oscillations ($\dot{p} = 0$).

Therefore, the reference currents can be written as

$$i_{\alpha}^* = \frac{2}{3} \left(\frac{v_{\alpha}^+ - v_{\alpha}^-}{(V^+)^2 - (V^-)^2} P^* + \frac{v_{\beta}^+ + v_{\beta}^-}{(V^+)^2 + (V^-)^2} Q^* \right) \quad (9)$$

$$i_{\beta}^* = \frac{2}{3} \left(\frac{v_{\beta}^+ - v_{\beta}^-}{(V^+)^2 - (V^-)^2} P^* - \frac{v_{\alpha}^+ + v_{\alpha}^-}{(V^+)^2 + (V^-)^2} Q^* \right) \quad (10)$$

and can be expressed as [59]

$$i_{\alpha}^* = I_p^+ \left(\frac{v_{\alpha}^+}{V^+} \right) - I_p^- \left(\frac{v_{\alpha}^-}{V^-} \right) + I_q^+ \left(\frac{v_{\beta}^+}{V^+} \right) + I_q^- \left(\frac{v_{\beta}^-}{V^-} \right) \quad (11)$$

$$i_{\beta}^* = I_p^+ \left(\frac{v_{\beta}^+}{V^+} \right) - I_p^- \left(\frac{v_{\beta}^-}{V^-} \right) - I_q^+ \left(\frac{v_{\alpha}^+}{V^+} \right) - I_q^- \left(\frac{v_{\alpha}^-}{V^-} \right) \quad (12)$$

where the current amplitudes (I_p^+ , I_p^- , I_q^+ and I_q^-) are formulated based on the following relations:

$$I_p^+ = \frac{2}{3} \frac{V^+}{(V^+)^2 - (V^-)^2} P^* \quad , \quad I_p^- = \frac{2}{3} \frac{V^-}{(V^+)^2 - (V^-)^2} P^* \quad (13)$$

$$I_q^+ = \frac{2}{3} \frac{V^+}{(V^+)^2 + (V^-)^2} Q^* \quad , \quad I_q^- = \frac{2}{3} \frac{V^-}{(V^+)^2 + (V^-)^2} Q^* \quad (14)$$

Details on the derivation of the reference powers (P^* and Q^*) can be found in the literature [25].

4. Experimental Results

Only the injection of P and Q into the grid was evaluated in the literature [25], but the effect that its control algorithm has on the voltage support was not considered. Hence, this effect on local voltages during a voltage sag will be the major focus of the present study, but in a more complex scenario of multiple grid-connected inverters. To this end, five experiments were performed using an experimental prototype (at the PNL) that emulates the operation of multiple renewable distributed generators based on inverters. Table 4 shows the values of the system parameter.

Table 4. System parameters.

Quantity	Acronym	Value
grid voltage	V	110.0 V rms
grid frequency	f	60.0 Hz
rated power	S_b	1.5 kVA
rated current	I_{rated}	5.0 A
LC filter inductances	L_f	5.0 mH
LC filter capacitances	C_f	1.5 μ F
LC filter damping resistors	R_d	68.0 Ω
Common resistive load	R_L	22.0 Ω
Local resistive loads	R_{L1}, R_{L3}	88.0 Ω
sampling/switching frequency	f_s	10.0 kHz

Different profiles of power injection have been tested—according to the power generated by each DPGS—using the concept of the network topology presented in Figure 1. All values of generated power (P_G), reference active power (P^*), and reference reactive power (Q^*), are consolidated in Table 5.

Table 5. Power injection profiles. P_G —generated power; P^* —reference active power; Q^* —reference reactive power.

Power	DPGS	Profile 1	Profile 2	Profile 3	Profile 4	Profile 5
P_G (W)	1	325.0	100.0	600.0	100.0	1000.0
	2	325.0	300.0	300.0	100.0	100.0
	3	325.0	300.0	300.0	100.0	100.0
	4	325.0	600.0	100.0	1000.0	100.0
P^* (W)	1	325.0	100.0	600.0	100.0	817.8
	2	325.0	300.0	300.0	100.0	100.0
	3	325.0	300.0	300.0	100.0	100.0
	4	325.0	600.0	100.0	780.9	100.0
Q^* (VAr)	1	898.0	935.3	669.5	937.2	0.0
	2	848.8	842.7	846.7	903.0	881.3
	3	800.2	801.5	810.2	856.2	846.5
	4	786.6	541.7	851.7	0.0	841.7

4.1. Operation of Multiple Grid-Connected Inverters

A balanced profile of power injection has been chosen to explain the experimental results obtained regarding the operation of multiple grid-connected inverters. In this profile, all the DPGSs have the same generated power ($P_{Gi} = 325.0$ W), and almost identical values of Q^* are obtained. Under these circumstances, it is possible to see the effect of the equivalent impedance on the voltage support capability at each node. Later it will be verified for this case that $P^* = P_G$.

Figure 3 shows the phase voltages of each DPGS, in which a 0.19-s voltage sag can be observed. A voltage sag threshold of 90% of the declared voltage [60] has been specified to detect the start and end

of the sag. At $t = 0.10$ s, the fault occurs but the control algorithm, together with the current limitation algorithm, is not yet enabled. At this time, the set of positive- and negative-sequence reference active currents focuses on maintaining the pre-fault power delivery. At $t = 0.22$ s, the control, together with the current limitation algorithm, is activated to appreciate its control action. The voltage recovers the pre-fault conditions from the instant $t = 0.32$ s, once the fault is cleared. The continuous red vertical lines enclose the region where the control is activated.

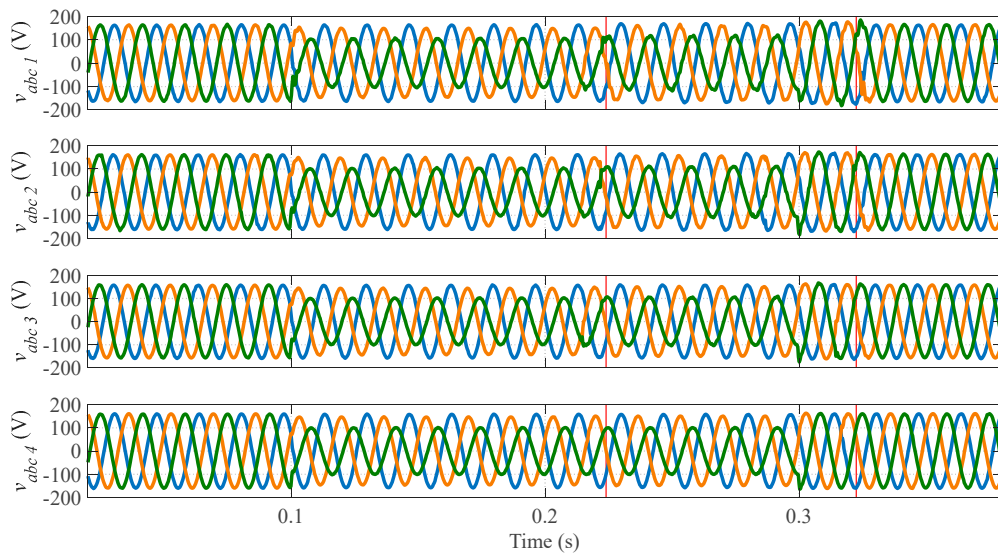


Figure 3. Experimental phase voltages with profile 1. v_a (blue), v_b (orange), and v_c (green).

Although the voltage sag and the phase voltage unbalance can be seen in Figure 3, the control action is easier to observe in Figure 4, in which the voltage sequence amplitudes are presented. The upper subfigure reveals that there has been a marked increase in the positive-sequence voltage amplitudes. However, the lower subfigure shows that the negative-sequence voltage amplitudes have hardly changed as a result of the amounts of I_{qi}^- that are injected.

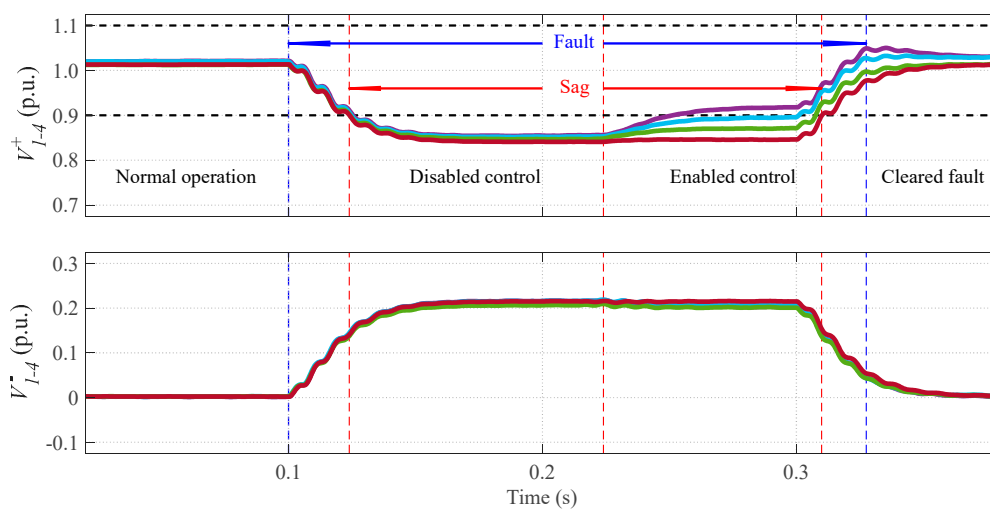


Figure 4. Voltage sequence amplitudes with profile 1. DPGS₁ (violet), DPGS₂ (sky-blue), DPGS₃ (emerald), and DPGS₄ (burgundy).

The characteristics of the fault are also clearly indicated. The dashed blue vertical lines show the duration of the failure ($0.10 < t < 0.32$ s), while the red lines delimit only the voltage sag below the specified threshold and denote the sector where the control algorithm is enabled. The dashed black horizontal lines indicate the upper and lower voltage thresholds.

Figure 5 shows the behavior of the current amplitudes (I_p^+ , I_p^- , I_q^+ and I_q^-). In normal operation, and after the fault is cleared, each DPGS only injects active power via positive sequence (I_p^+). During the first half of the voltage sag, only active power is injected through both sequences (I_p^+ and I_p^-). The reactive current injection (RCI) is enabled from the instant $t = 0.22$ s. Note that the four components (I_p^+ , I_p^- , I_q^+ and I_q^-) are only injected when the control is enabled.

Figure 6 shows how the experimental phase currents increase thanks to the control action, but without exceeding the nominal value. The black dashed lines represent the maximum current that can be injected by each DPGS. When the control is enabled during the voltage sag, $i_c = I_{rated}$ (5 A). Note that I_{max} is reached in the most dropped phase (see v_c in Figure 3).

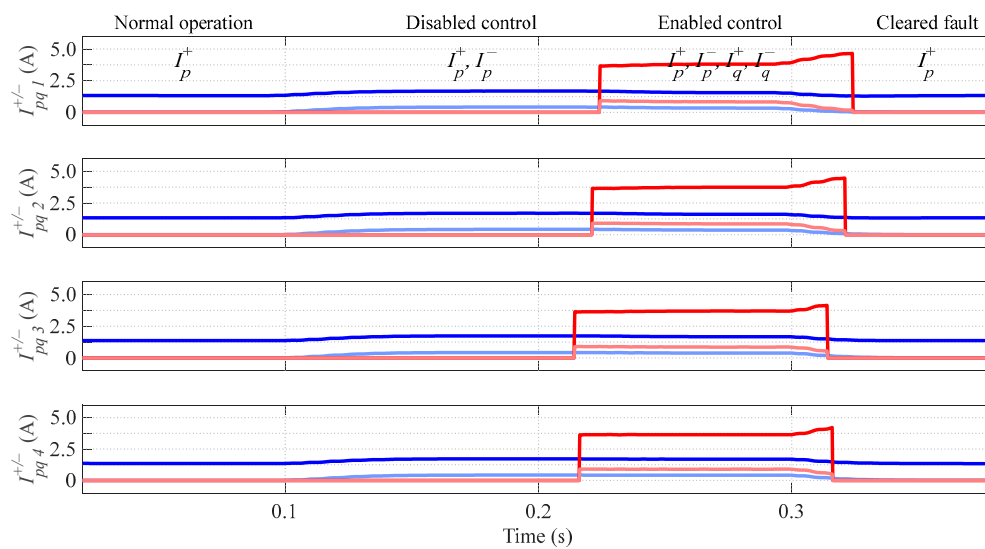


Figure 5. Current sequences with profile 1. Positive-sequence active current I_p^+ (blue), negative-sequence active current I_p^- (light blue), positive-sequence reactive current I_q^+ (red), and negative-sequence reactive current I_q^- (light red).

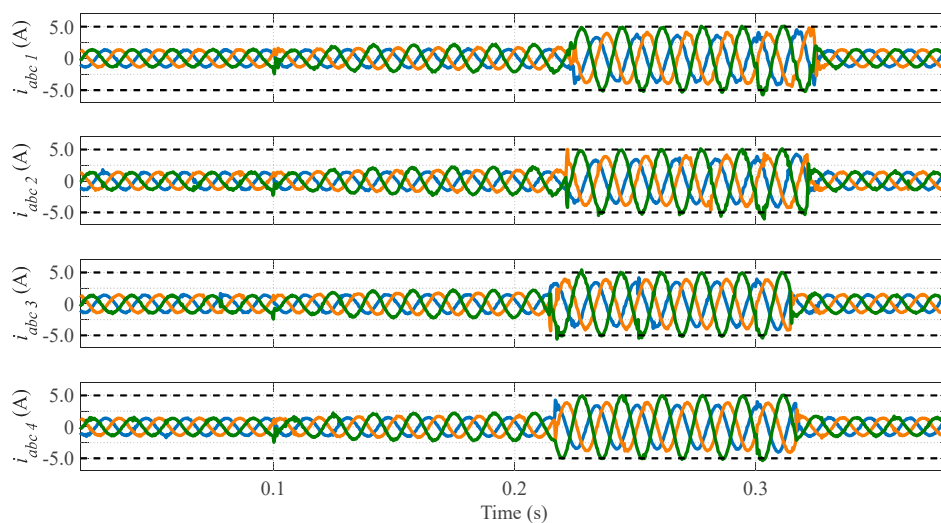


Figure 6. Experimental phase currents with profile 1. i_a (blue), i_b (orange), and i_c (green).

Figure 7 displays the power delivered to the network by each DPGS. In the top subfigure, it can be seen that the instantaneous active power (p) is free of oscillations. The opposite occurs with the instantaneous reactive power (q) that exhibits oscillations at twice the network frequency, as seen in the lower subfigure.

This profile corresponds to a low-power production scenario in which $P^* = P_G$. The DPGSs inject the same amount of active power, but there are small differences between the amounts of reactive power they inject into the network. Although the voltage sag programmed as the fault in the three-phase Pacific AMX-360 AC source has a constant profile, each node sees a slightly different voltage sag as a result of its propagation. Consequently, the calculation of Q^* at each node varies according to the measurement of the voltage sag characteristics (V^+ , V^- and ϕ).

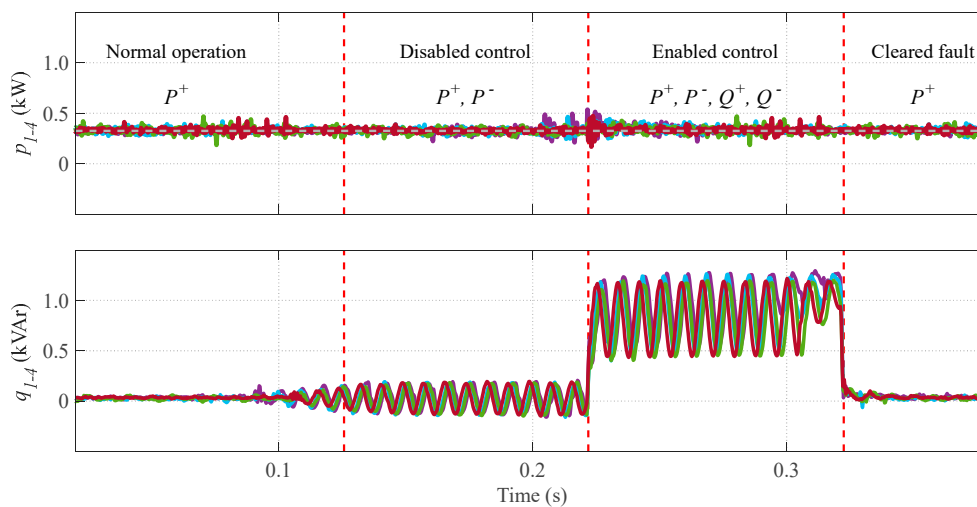


Figure 7. Experimental measured powers with profile 1. DPGS₁ (violet), DPGS₂ (sky-blue), DPGS₃ (emerald), and DPGS₄ (burgundy).

4.2. Experimental Analysis of the Voltage Support Capability

The five power injection profiles listed in Table 5 are analyzed concerning the variations of the collective rms value of the grid voltage at each DPGS. The equivalent impedance plays an essential role in this evaluation because its effect is amplified when the control algorithm is activated during the grid failure.

The experimental results of each test are presented in two subfigures. The effective voltages are shown in the left subfigure. The dashed red vertical lines delimit the zone where the control is enabled, and the dashed black horizontal line indicates the voltage sag threshold of 90% of the declared voltage. The bar graph gives information on the voltage variation at each node during the voltage sag; the light-colored left bar represents V_{ei} when the control is disabled, and the dark-colored right bar depicts V_{ei} when the control is enabled. Besides, the four equivalent impedance values listed in Table 2 are indicated at the top of each figure. They are expressed in polar form to quickly identify the network behavior according to the impedance angle (θ_{eqi}).

4.2.1. Power Injection Profile 1

Figure 8 displays the operation of the network according to the first power injection profile, considering $P_{Gi} = 325.0$ W (low-production scenario). The P injection is not suspended during the voltage sag; the controller gives priority to this injection. Therefore, the voltage increase is due to the Q injection in the interval $0.22 < t < 0.32$ s. As $P_{Gi} < P_{maxi}$, then $P^*_i = P_{Gi} = 325.0$ W, and a considerable injection of reactive power Q^* is produced. This injection maximizes the voltage support in all the network nodes, but mainly in those that see a high equivalent inductance. This explanation

agrees with the results presented in Figure 4, in which an increase in the positive-sequence voltage amplitudes is observed. The node corresponding to the DPGS 4 has the smallest equivalent inductance ($L_{eq4} = 0.6$ mH) of the testbed and, therefore, its voltage support is lower.

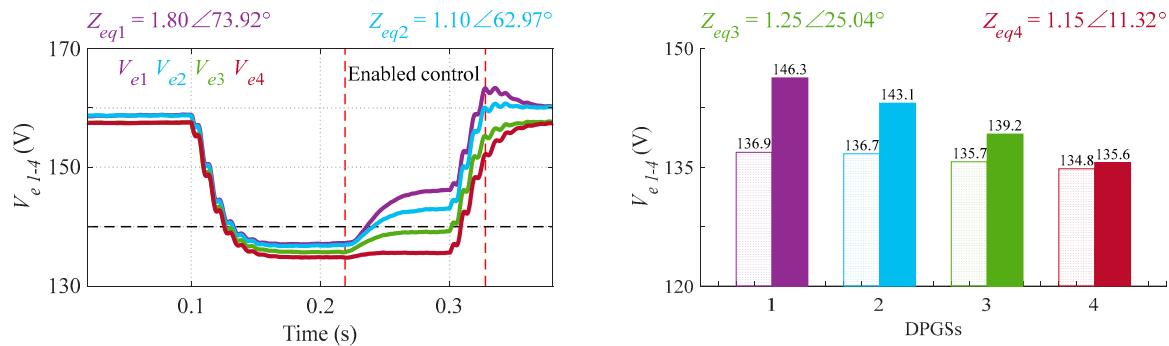


Figure 8. Effective voltages with profile 1.

4.2.2. Power Injection Profile 2

Figure 9 shows the operation of the network according to the second power injection profile. Since $P_{Gi} < P_{maxi}$, then $P^*_i = P_{Gi}$. This change of profile did not affect the performance of the DPGSs. Although P^*_2 and P^*_3 present the same power reduction (from 325.0 W to 300.0 W), the DPGSs 2 and 3 have values of Q^* very similar to those of the previous profile. However, the DPGS 1, which increased its value of Q^* , and the DPGS 4, which doubled its amount of P_G , did improve their voltage support capability. Note also that, although $R_{eq3} = R_{eq4} = 1.13 \Omega$, the DPGS 3 performs better voltage support than the DPGS 4, because $L_{eq3} = \frac{7}{3}L_{eq4}$.

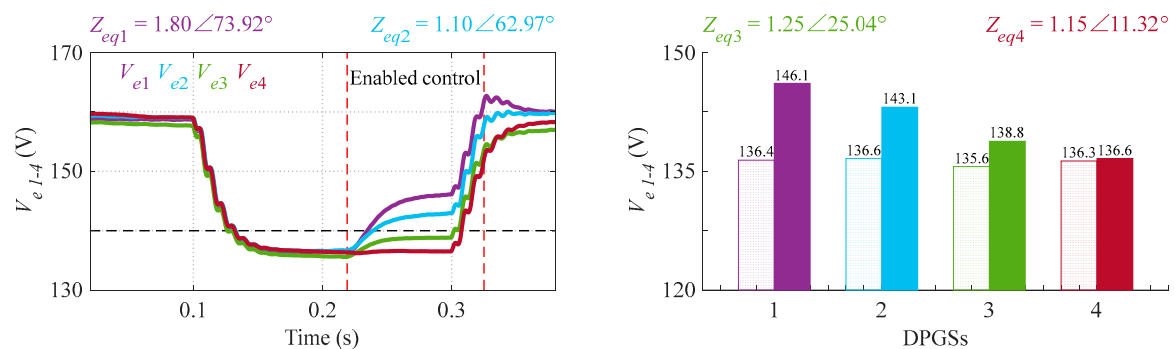


Figure 9. Effective voltages with profile 2.

4.2.3. Power Injection Profile 3

The operation of the network according to the power injection profile 3 is shown in Figure 10. As in the previous profiles, $P_{Gi} < P_{maxi}$ and, therefore, $P^*_i = P_{Gi}$. The DPGSs 2 and 3 maintain the same values of P^* (300.0 W) and, therefore, the values of Q^* are similar to those of the previous profile. Now, the DPGS 1 injects 600.0 W of active power into the network, which is why the effective voltage (V_{e1}) at this node is the least affected during the voltage sag. However, in this profile, the voltage variation ΔV_{e1} is lower than in the previous one ($\Delta V_{e1}^{PIP3} < \Delta V_{e1}^{PIP2}$). If Q^* decreases because of a higher P^* , the voltage support capability also decreases. In this test, the effective voltage V_{e4} is the most affected when the fault occurs. The equivalent impedance seen by the DPGS 4 is dominantly resistive, and its generated power is the lowest ($P^*_4 = P_{G4} = 100.0$ W). The value of Q^*_4 is high, but its effect on the voltage support is reduced.

It should be noted that active power references depend on the amount of generated power, as opposed to the reactive power references. Therefore, in a low-power production scenario, the possibilities of adjusting active power references are reduced.

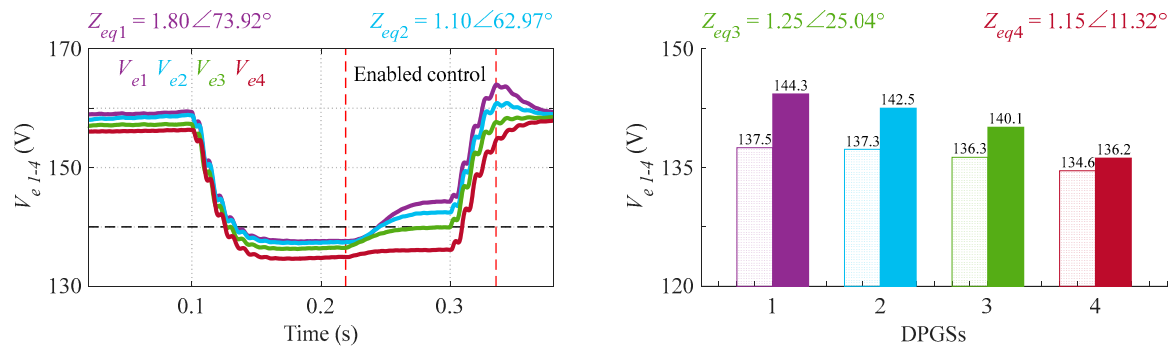


Figure 10. Effective voltages with profile 3.

4.2.4. Power Injection Profile 4

Figure 11 shows the operation of the network according to the fourth power injection profile. A low-power production scenario has been configured for the DPGSs 1 to 3 ($P_G = 100.0$ W), which causes a high injection of reactive power Q^* that mainly benefits the nodes 1 and 2. The opposite occurs with the DPGS 4, which has a high active power production ($P_{G4} = 1000.0$ W) that makes the reactive power reference zero ($Q^*_4 = 0.0$ VAR).

The equivalent impedance Z_{eq4} seen by the DPGS 4 allows appreciating the significant effect that the P injection has on the voltage support in resistive grids. Since the amplitude of the grid voltage decreases during the grid fault, the generated reference currents, which focus on maintaining the pre-fault power delivery, overpasses the limit value in the interval $0.10 < t < 0.22$ s. At $t = 0.22$ s, the control, together with the current limitation algorithm, is activated, which makes the currents remain below the maximum admissible value, while the maximum active power is injected into the grid ($P^*_4 = P_{max4} = 780.9$ W). As soon as the control is enabled, the APC is performed, that is, the components of the active currents (I_{p4}^+ and I_{p4}^-) are reduced. This control action can be seen reflected in the behavior of the effective voltage V_{e4} .

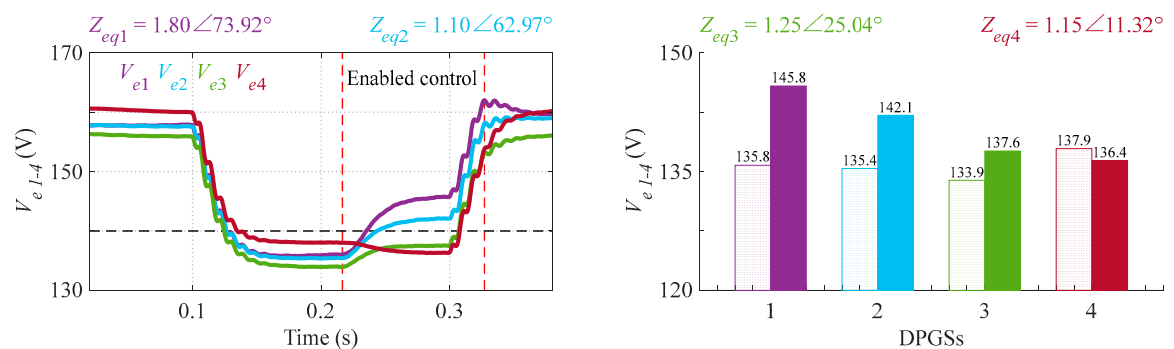


Figure 11. Effective voltages with profile 4.

4.2.5. Power Injection Profile 5

The results of the voltage support effect of the last power injection profile are presented in Figure 12. In this case, the low-power production scenario was configured for the DPGSs 2 to 4 ($P_G = 100.0$ W). Now, the DPGS 1 has a high active power production ($P_{G1} = 1000.0$ W) that reduces the reactive power reference at this node to zero ($Q^*_1 = 0.0$ VAR).

This profile of power injection is the least efficient regarding voltage support, except at the node 2, which undergoes the most notable voltage change (ΔV_{e2}) of the profile. The equivalent impedance Z_{eq2} seen by the DPGS 2, together with its reference of reactive power (Q^*_2) when the control is enabled, maximizes the effective voltage variation. Now, the DPGS 1 performs the APC (from 1000.0 W to 817.8 W) when the voltage sag occurs. Observe that $P^*_1 < P_{G1}$ because $P_{G1} > P_{max1}$ during the failure. Therefore, the current amplitudes I_{p1}^+ and I_{p1}^- are reduced, but the effective voltage V_{e1} improves when the control is activated because of ΔV_{e2} . Considering the characteristics of Z_{eq1} , the reduction of P^*_1 is important to control I_{max1} , but its effect on the voltage support is negligible.

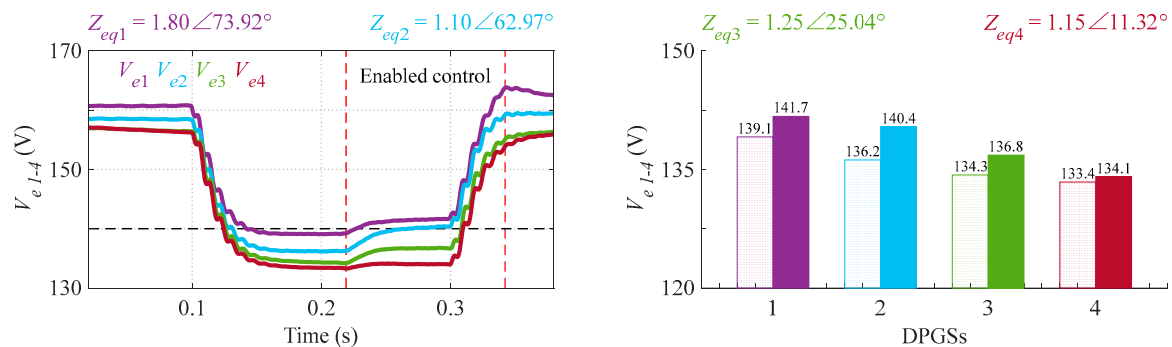


Figure 12. Effective voltages with profile 5.

4.3. Discussion on Voltage Support Capabilities

Figure 13 shows the results of the voltage support capability of the DPGS 1 during the five tests that were carried out. At this point, it is not necessary to analyze each DPGS, thus a single one has been chosen to discuss its behavior. The primary variables have been normalized and are presented in a single plane in per unit (p.u.). The maximum values obtained during each test are displayed using circular markers. The gray markers indicate the effective voltage (V_{e1}) when the control is disabled (DisC), the black ones indicate the value of this voltage when the control is enabled (EnC), and the green ones represent its variation (ΔV_{e1}). Finally, the blue and red markers indicate the active and reactive power references, respectively, when the control is enabled (EnC).

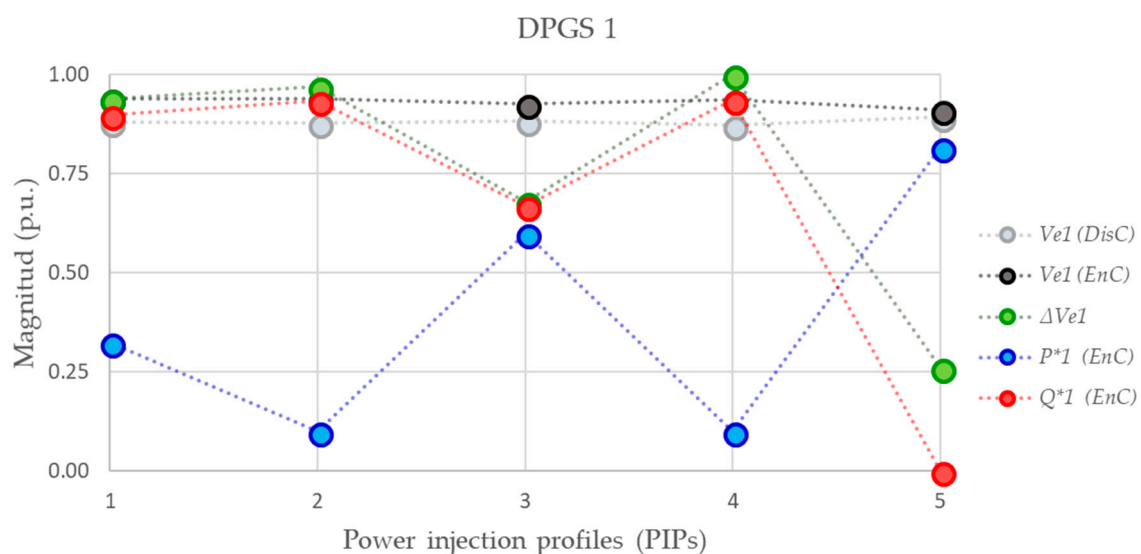


Figure 13. The DPGS 1 and its voltage support capability. DisC—control is disabled; EnC—control is enabled; ΔV_{e1} —variation of voltage.

Considering the equivalent impedance Z_{eq1} seen by the DPGS 1, in this case, the injection of reactive power (Q) has a very noticeable effect on the voltage support; the profiles 1, 2, and 4 confirm this fact. On the contrary, the voltage support is minimized when the injection of active power (P) is predominant; the profile 5 is a clear example. Thus, for the profiles 3 and 5 that have sufficient generated power ($P_{G1}^{PIP3} = 600.0$ W and $P_{G1}^{PIP5} = 1000.0$ W), it would have been better not only to inject Q , but also to inject a certain amount of P to achieve more appropriate voltage support considering the equivalent impedance Z_{eq1} . The impedance angle θ_{eq1} directly marks the criteria to establish the relationship between P and Q .

In general, the grid impedance is considered mainly inductive ($\theta \approx 90^\circ$), but in low-voltage networks, the grid impedance is mainly resistive ($\theta \approx 0^\circ$) [57]. In this work, a mixed case has been considered in which the equivalent impedance seen by each inverter has inductive and resistive characteristics.

Given that the equivalent impedance seen by the DPGSs 1 and 2 is mainly inductive, based on the experiments carried out in this work, it would be appropriate for these two inverters only to inject I_q^+ . The injection of I_q^- could be discarded as its effect on the negative-sequence voltage amplitude V^- is almost imperceptible (see Figure 4). In the same way, the equivalent impedance seen by the DPGSs 3 and 4 is mainly resistive, which is why the maximum injection of active power during the voltage sag will help to support the grid better; however, when the generated power P_G is deficient, reactive power must necessarily be injected. In the fourth power injection profile, the DPGS 4 has a high active power production and need not inject reactive power during the fault, as explained in Section 4.2.4.

It should be noted that if only the injection of I_q^+ is considered, then the voltage in each phase rises equally [18], balanced phase currents are achieved, and the instantaneous active power exhibits oscillations at twice the network frequency.

If only reactive power (Q) is injected into a mainly resistive network when a voltage sag occurs, the injection has no effect on the voltage support, but it produces power losses due to core losses and copper losses ($P = I_{rms}^2 R$) [61]. Similarly, when active power (P) is injected into a mainly inductive network, the injection also has no effect on the local voltages and, besides, limits the injection capability of the inverter.

This analysis allows asserting that if I_p^+ is injected into an inductive network when a voltage sag occurs, the voltage support is inefficient; likewise, that if I_q^+ is injected when a voltage sag occurs in a resistive network, the reactive current injection does not mitigate the sag, but there are power losses.

4.4. Future Works

In future works, not only experimental tests will be carried out with multiple converters simultaneously injecting active and reactive power into the grid, but different injection strategies will also be tested. In the same way, different indexes of performance will be measured, compared, and analyzed, among which it is essential to highlight the following: injected current, positive-sequence voltage, negative-sequence voltage, voltage imbalance, injected active power, and injected reactive power. Moreover, both voltage support and grid feeding have to be further evaluated.

5. Conclusions

Many solutions have been adopted to control a single inverter with different control strategies; however, new analysis factors appear—which have not been observed in previous works—when several grid-connected inverters coincide.

In this work, a specific control algorithm has been chosen for all inverters, and two main parameters have been considered to perform the analysis presented in the previous section: (1) the equivalent impedances (Z_{eqi}) and (2) the generated power (P_{Gi}). The different profiles of active power production provide a grid environment of variable conditions. The changes in these profiles have a direct impact on the power delivery settings for each DPGS.

The principle used with a single inverter to regulate the grid voltages through the injection of reactive current has been verified experimentally in several inverters connected to a network with complex impedance. In addition, each controller can simultaneously deliver active and reactive power to the network through positive- and negative-sequence components.

Although the literature has documented the use of reactive power control methods to deal with overvoltage problems taking advantage of the power capabilities of distributed inverters, this study demonstrates experimentally that these capabilities can also be used to support the grid under voltage sags in a more complex scenario.

It is essential to include the grid impedance effect when designing or selecting a control strategy for DG systems. The impedance angle will delimit the injection method, and the impedance module will determine the effect/impact of such injection.

If the local voltages are within the stipulated limits, no action will be necessary. Otherwise, each DPGS will execute its control strategy according to the interests of the owners and transmission system operators (TSOs) and, ideally, as a function of the equivalent impedance seen by each converter, an exciting topic of research that is open for a new generation of GCs. The obtained experimental results invite to continue with the investigation of the dynamics that arise in the grid when multiple converters simultaneously inject power and help support this grid in the presence of faults such as voltage sags.

Author Contributions: This paper has been jointly developed by all authors. The authors participated in the comparative analysis, and in the obtaining and discussion of the experimental results, as well as in the writing of the article.

Funding: This work has been supported by ELAC2014/ESE0034 from the European Union and its linked Spanish national project PCIN-2015-001. We also appreciate the support from the Ministry of Economy and Competitiveness of Spain and European Regional Development Fund (FEDER) under projects ENE2015-64087-C2-1-R.

Conflicts of Interest: The authors declare no conflict of interest.

References

1. Katti, P.K.; Khedkar, M.K. Integrated operation of decentralised resources for rural area power supply applications. In Proceedings of the 2005 IEEE/PES Transmission & Distribution Conference & Exposition: Asia and Pacific, Dalian, China, 18 August 2005.
2. Blaabjerg, F.; Teodorescu, R.; Liserre, M.; Timbus, A.V. Overview of Control and Grid Synchronization for Distributed Power Generation Systems. *IEEE Trans. Ind. Electron.* **2006**, *53*, 1398–1409. [CrossRef]
3. Troester, E. New German Grid Codes for Connecting PV Systems to the Medium Voltage Power Grid. Available online: https://scholar.google.es/scholar?cluster=5874071522966012685&hl=es&as_sdt=0,5&as_vis=1 (accessed on 25 July 2018).
4. Tsili, M.; Papathanassiou, S. A review of grid code technical requirements for wind farms. *IET Renew. Power Gener.* **2009**, *3*, 308–332. [CrossRef]
5. Altin, M.; Goksu, O.; Teodorescu, R.; Rodriguez, P.; Jensen, B.-B.; Helle, L. Overview of recent grid codes for wind power integration. In Proceedings of the 2010 12th International Conference on Optimization of Electrical and Electronic Equipment, Basov, Romania, 20–22 May 2010; pp. 1152–1160.
6. Yang, Y.; Enjeti, P.; Blaabjerg, F.; Wang, H. Wide-Scale Adoption of Photovoltaic Energy: Grid Code Modifications Are Explored in the Distribution Grid. *IEEE Ind. Appl. Mag.* **2015**, *21*, 21–31. [CrossRef]
7. *Waveform Characteristics of Voltage Sags: Statistical Analysis*; TR-112692; EPRI: Palo Alto, CA, USA, 1999.
8. Smith, J.C.; Hensley, G.; Ray, L. *IEEE Recommended Practice for Monitoring Electric Power Quality*; IEEE Standards Association: Piscataway, NJ, USA, 1995.
9. Teodorescu, R.; Liserre, M.; Rodríguez, P. Grid Requirements for PV. In *Grid Converters for Photovoltaic and Wind Power Systems*; John Wiley & Sons, Ltd.: Chichester, UK, 2010; pp. 31–42.
10. Teodorescu, R.; Liserre, M.; Rodríguez, P. Grid Requirements for WT Systems. In *Grid Converters for Photovoltaic and Wind Power Systems*; John Wiley & Sons, Ltd.: Chichester, UK, 2010; pp. 145–167.
11. Sourkounis, C.; Tourou, P. Grid Code Requirements for Wind Power Integration in Europe. *Conf. Pap. Energy* **2013**, *2013*, 437674. [CrossRef]

12. Uphues, A.; Notzold, K.; Griessel, R.; Wegener, R.; Soter, S. Overview of LVRT-capability pre-evaluation with an inverter based test bench. In Proceedings of the 2015 IEEE 24th International Symposium on Industrial Electronics (ISIE), Buzios, Brazil, 3–5 June 2015.
13. Teodorescu, R.; Liserre, M.; Rodríguez, P. Islanding Detection. In *Grid Converters for Photovoltaic and Wind Power Systems*; John Wiley & Sons, Ltd.: Chichester, UK, 2010; pp. 93–122.
14. Alepuz, S.; Busquets-Monge, S.; Bordonau, J.; Martinez-Velasco, J.A.; Silva, C.A.; Pontt, J.; Rodriguez, J. Control Strategies Based on Symmetrical Components for Grid-Connected Converters Under Voltage Dips. *IEEE Trans. Ind. Electron.* **2009**, *56*, 2162–2173. [[CrossRef](#)]
15. Wang, F.; Duarte, J.L.; Hendrix, M.A. Pliant Active and Reactive Power Control for Grid-Interactive Converters Under Unbalanced Voltage Dips. *IEEE Trans. Power Electron.* **2011**, *26*, 1511–1521. [[CrossRef](#)]
16. Camacho, A.; Castilla, M.; Miret, J.; Vasquez, J.C.; Alarcón-Gallo, E. Flexible Voltage Support Control for Three-Phase Distributed Generation Inverters Under Grid Fault. *IEEE Trans. Ind. Electron.* **2013**, *60*, 1429–1441. [[CrossRef](#)]
17. Miret, J.; Camacho, A.; Castilla, M.; García de Vicuña, J.L.; Matas, J. Control Scheme With Voltage Support Capability for Distributed Generation Inverters Under Voltage Sags. *IEEE Trans. Power Electron.* **2013**, *28*, 5252–5262. [[CrossRef](#)]
18. Camacho, A.; Castilla, M.; Miret, J.; Guzman, R.; Borrell, A. Reactive Power Control for Distributed Generation Power Plants to Comply With Voltage Limits During Grid Faults. *IEEE Trans. Power Electron.* **2014**, *29*, 6224–6234. [[CrossRef](#)]
19. Miret, J.; Castilla, M.; Camacho, A.; García de Vicuña, J.L.; Matas, J. Control Scheme for Photovoltaic Three-Phase Inverters to Minimize Peak Currents During Unbalanced Grid-Voltage Sags. *IEEE Trans. Power Electron.* **2012**, *27*, 4262–4271. [[CrossRef](#)]
20. Rodriguez, P.; Luna, A.; Hermoso, J.R.; Etxeberria-Otadui, I.; Teodorescu, R.; Blaabjerg, F. Current control method for distributed generation power generation plants under grid fault conditions. In Proceedings of the IECON 2011—37th Annual Conference of the IEEE Industrial Electronics Society, Melbourne, VIC, Australia, 7–10 November 2011; pp. 1262–1269.
21. Rodriguez, P.; Medeiros, G.; Luna, A.; Cavalcanti, M.C.; Teodorescu, R. Safe current injection strategies for a STATCOM under asymmetrical grid faults. In Proceedings of the 2010 IEEE Energy Conversion Congress and Exposition, Atlanta, GA, USA, 12–16 September 2010; pp. 3929–3935.
22. Suul, J.A.; Luna, A.; Rodriguez, P.; Undeland, T. Virtual-Flux-Based Voltage-Sensor-Less Power Control for Unbalanced Grid Conditions. *IEEE Trans. Power Electron.* **2012**, *27*, 4071–4087. [[CrossRef](#)]
23. Lee, C.-T.; Hsu, C.-W.; Cheng, P.-T. A Low-Voltage Ride-Through Technique for Grid-Connected Converters of Distributed Energy Resources. *IEEE Trans. Ind. Appl.* **2011**, *47*, 1821–1832. [[CrossRef](#)]
24. Camacho, A.; Castilla, M.; Miret, J.; Borrell, A.; García de Vicuña, J.L. Active and Reactive Power Strategies With Peak Current Limitation for Distributed Generation Inverters During Unbalanced Grid Faults. *IEEE Trans. Ind. Electron.* **2015**, *62*, 1515–1525. [[CrossRef](#)]
25. Sosa, J.L.; Castilla, M.; Miret, J.; Matas, J.; Al-Turki, Y.A. Control Strategy to Maximize the Power Capability of PV Three-Phase Inverters During Voltage Sags. *IEEE Trans. Power Electron.* **2016**, *31*, 3314–3323. [[CrossRef](#)]
26. Tang, C.; Chen, Y.-T.; Chen, Y. PV Power System With Multi-Mode Operation and Low-Voltage Ride-Through Capability. *IEEE Trans. Ind. Electron.* **2015**, *62*, 7524–7533. [[CrossRef](#)]
27. Chen, H.-C.; Lee, C.-T.; Cheng, P.-T.; Teodorescu, R.; Blaabjerg, F. A Low-Voltage Ride-Through Technique for Grid-connected Converters with Reduced Power Transistors Stress. *IEEE Trans. Power Electron.* **2016**, *31*, 8562–8571. [[CrossRef](#)]
28. Mozumder, S.; Dhar, A.; Rangarajan, S.S.; Karthikeyan, S.P. Coordinated operation of multiple inverter based renewable distributed generators as an active power injector and reactive power compensator. In Proceedings of the 2014 International Conference on Computation of Power, Energy, Information and Communication (ICCPIC), Chennai, India, 16–17 April 2014; pp. 298–303.
29. Lee, Y.-D.; Park, S.-Y. Reactive power allocation control scheme for multiple grid connected inverters. In Proceedings of the 2015 9th International Conference on Power Electronics and ECCE Asia (ICPE-ECCE Asia), Seoul, Korea, 1–5 June 2015; pp. 2481–2488.
30. Velasco, M.; Martí, P.; Torres-Martínez, J.; Miret, J.; Castilla, M. On the optimal reactive power control for grid-connected photovoltaic distributed generation systems. In Proceedings of the IECON 2015—41st Annual Conference of the IEEE Industrial Electronics Society, Yokohama, Japan, 9–12 November 2015.

31. Momeneh, A.; Castilla, M.; Miret, J.; Martí, P.; Velasco, M. Comparative study of reactive power control methods for photovoltaic inverters in low-voltage grids. *IET Renew. Power Gener.* **2016**, *10*, 310–318. [[CrossRef](#)]
32. Martí, P.; Velasco, M.; Torres-Martínez, J.; Miret, J.; Castilla, M. Reactive power control for loss minimization in low-voltage distributed generation systems. In Proceedings of the 2016 12th IEEE International Conference on Control and Automation (ICCA), Kathmandu, Nepal, 1–3 June 2016; pp. 371–376.
33. Kulkarni, O.V.; Doolla, S.; Fernandes, B.G. Mode Transition Control Strategy for Multiple Inverter-Based Distributed Generators Operating in Grid-Connected and Standalone Mode. *IEEE Trans. Ind. Appl.* **2017**, *53*, 5927–5939. [[CrossRef](#)]
34. Miret, J.; García de Vicuña, J.L.; Guzmán, R.; Camacho, A.; Ghahderijani, M.M. A Flexible Experimental Laboratory for Distributed Generation Networks Based on Power Inverters. *Energies* **2017**, *10*, 1589. [[CrossRef](#)]
35. Demirok, E.; González, P.C.; Frederiksen, K.H.B.; Sera, D.; Rodriguez, P.; Teodorescu, R. Local Reactive Power Control Methods for Overvoltage Prevention of Distributed Solar Inverters in Low-Voltage Grids. *IEEE J. Photovolt.* **2011**, *1*, 174–182. [[CrossRef](#)]
36. Camacho, A.; Castilla, M.; Canziani, F.; Moreira, C.; Coelho, P.; Gomes, M.; Mercado, P. Performance Comparison of Grid-Faulty Control Schemes for Inverter-Based Industrial Microgrids. *Energies* **2017**, *10*, 2096. [[CrossRef](#)]
37. Zhao, X.; Guerrero, J.M.; Savaghebi, M.; Vasquez, J.C.; Wu, X.; Sun, K. Low-Voltage Ride-Through Operation of Power Converters in Grid-Interactive Microgrids by Using Negative-Sequence Droop Control. *IEEE Trans. Power Electron.* **2017**, *32*, 3128–3142. [[CrossRef](#)]
38. Teodorescu, R.; Liserre, M.; Rodríguez, P. Grid synchronization in three-phase power converters. In *Grid Converters for Photovoltaic and Wind Power Systems*; John Wiley & Sons, Ltd.: Chichester, UK, 2010; pp. 169–204.
39. Teodorescu, R.; Liserre, M.; Rodríguez, P. Control of grid converters under grid faults. In *Grid Converters for Photovoltaic and Wind Power Systems*; John Wiley & Sons, Ltd.: Chichester, UK, 2010; pp. 237–287.
40. Blackburn, J.L.; Domin, T.J. Introduction and General Philosophies. In *Protective Relaying: Principles and Applications*, 3rd ed.; CRC Press: Boca Raton, FL, USA, 2006.
41. Anderson, P.M. Symmetrical Components. In *Analysis of Faulted Power Systems*, 1st ed.; Wiley-IEEE Press: New York, NY, USA, 1995.
42. Anderson, P.M. Analysis of unsymmetrical faults: Three-component method. In *Analysis of Faulted Power Systems*, 1st ed.; Wiley-IEEE Press: New York, NY, USA, 1995.
43. Blackburn, J.L.; Domin, T.J. Symmetrical components: A review. In *Protective Relaying: Principles and Applications*, 3rd ed.; CRC Press: Boca Raton, FL, USA, 2006.
44. Teodorescu, R.; Liserre, M.; Rodríguez, P. Appendix A: Space vector transformations of three-phase systems. In *Grid Converters for Photovoltaic and Wind Power Systems*; John Wiley & Sons, Ltd.: Chichester, UK, 2010; pp. 355–362.
45. Das, J.C. Symmetrical components using matrix methods. In *Understanding Symmetrical Components for Power System Modeling*; John Wiley & Sons, Inc.: Hoboken, NJ, USA, 2016; pp. 1–14.
46. Das, J.C. Fundamental concepts of symmetrical components. In *Understanding Symmetrical Components for Power System Modeling*; John Wiley & Sons, Inc.: Hoboken, NJ, USA, 2016; pp. 15–37.
47. Das, J.C. Unsymmetrical fault calculations. In *Understanding Symmetrical Components for Power System Modeling*; John Wiley & Sons, Inc.: Hoboken, NJ, USA, 2016; pp. 103–146.
48. *IEEE Standard Definitions for the Measurement of Electric Power Quantities Under Sinusoidal, Nonsinusoidal, Balanced, or Unbalanced Conditions*; IEEE Standards Association: Piscataway, NJ, USA, 2010.
49. Teodorescu, R.; Liserre, M.; Rodríguez, P. Appendix B: Instantaneous power theories. In *Grid Converters for Photovoltaic and Wind Power Systems*; John Wiley & Sons, Ltd.: Chichester, UK, 2010; pp. 363–379.
50. Braun, M.; Stetz, T.; Bründlinger, R.; Mayr, C.; Ogimoto, K.; Hatta, H.; Kobayashi, H.; Kroposki, B.; Mather, B.; Coddington, M.; Lynn, K.; et al. Is the distribution grid ready to accept large-scale photovoltaic deployment? State of the art, progress, and future prospects. *Prog. Photovolt. Res. Appl.* **2012**, *20*, 681–697. [[CrossRef](#)]
51. Akagi, H.; Watanabe, E.H.; Aredes, M. Electric power definitions: Background. In *Instantaneous Power Theory and Applications to Power Conditioning*; Akagi, H., Watanabe, E.H., Aredes, M., Eds.; John Wiley & Sons, Inc.: Hoboken, NJ, USA, 2017; pp. 17–36.

52. Camacho, A.; Castilla, M.; Miret, J.; García de Vicuña, J.L.; Guzman, R. Positive and Negative Sequence Control Strategies to Maximize the Voltage Support in Resistive–Inductive Grids During Grid Faults. *IEEE Trans. Power Electron.* **2018**, *33*, 5362–5373. [[CrossRef](#)]
53. Camacho, A.; Castilla, M.; Miret, J.; García de Vicuña, J.L.; Garnica López, M.A. Control Strategy for Distribution Generation Inverters to Maximize the Voltage Support in the Lowest Phase During Voltage Sags. *IEEE Trans. Ind. Electron.* **2018**, *65*, 2346–2355. [[CrossRef](#)]
54. Shabestary, M.M. A Comparative Analytical Study on Low-Voltage Ride-Through Reference-Current-Generation (LVRT-RCG) Strategies in Converter-Interfaced DER Units. Master’s Thesis, University of Alberta, Edmonton, AB, Canada, 2015.
55. Rodriguez, P.; Timbus, A.V.; Teodorescu, R.; Liserre, M.; Blaabjerg, F. Flexible Active Power Control of Distributed Power Generation Systems During Grid Faults. *IEEE Trans. Ind. Electron.* **2007**, *54*, 2583–2592. [[CrossRef](#)]
56. Ma, K.; Liserre, M.; Blaabjerg, F. Power controllability of three-phase converter with unbalanced AC source. In Proceedings of the 2013 Twenty-Eighth Annual IEEE Applied Power Electronics Conference and Exposition (APEC), Long Beach, CA, USA, 17–21 March 2013.
57. Guo, X.; Zhang, X.; Wang, B.; Wu, W.; Guerrero, J.M. Asymmetrical Grid Fault Ride-Through Strategy of Three-Phase Grid-Connected Inverter Considering Network Impedance Impact in Low-Voltage Grid. *IEEE Trans. Power Electron.* **2014**, *29*, 1064–1068. [[CrossRef](#)]
58. Rodriguez, F.J.; Bueno, E.; Aredes, M.; Rolim, L.G.B.; Neves, F.A.S.; Cavalcanti, M.C. Discrete-time implementation of second order generalized integrators for grid converters. In Proceedings of the 2008 34th Annual Conference of IEEE Industrial Electronics, Orlando, FL, USA, 10–13 November 2008.
59. Garnica López, M.A.; García de Vicuña, J.L.; Miret, J.; Castilla, M.; Guzmán, R. Control Strategy for Grid-Connected Three-Phase Inverters During Voltage Sags to Meet Grid Codes and to Maximize Power Delivery Capability. *IEEE Trans. Power Electron.* **2018**. [[CrossRef](#)]
60. *IEEE Guide for Voltage Sag Indices*; IEEE Standards Association: Piscataway, NJ, USA, 2014.
61. Sun, D.; Abe, S.; Shoults, R.R.; Chen, M.S.; Eichenberger, P.; Farris, D. Calculation of Energy Losses in a Distribution System. *IEEE Trans. Power Appar. Syst.* **1980**, *PAS-99*, 1347–1356. [[CrossRef](#)]



© 2018 by the authors. Licensee MDPI, Basel, Switzerland. This article is an open access article distributed under the terms and conditions of the Creative Commons Attribution (CC BY) license (<http://creativecommons.org/licenses/by/4.0/>).

4

Publication III:

PI-BASED CONTROLLER FOR LOW-POWER DISTRIBUTED INVERTERS TO MAXIMIZE REACTIVE CURRENT INJECTION WHILE AVOIDING OVER VOLTAGE DURING VOLTAGE SAGS

J. Miret, M. Garnica, M. Castilla, L. García de Vicuña, and A. Camacho, “PI-based controller for low-power distributed inverters to maximize reactive current injection while avoiding over voltage during voltage sags,” *IET Power Electron.*, *in press*.

ATTENTION;

You can consult the quoted article, included on pages 56 to 67 on the thesis, on the publisher's website <https://digital-library.theiet.org/content/journals/10.1049/iet-pel.2018.5071>

Summary

- 4.1 Introduction
 - 4.2 Grid-connected inverters under voltage sags
 - 4.3 Formulation of control objectives and proposed control algorithm
 - 4.4 Design guidelines for the control loops
 - 4.5. Experimental results
 - 4.6 Comparison to previous control schemes
 - 4.7. Conclusions
 - 4.8 References
-

5

Analysis of the results:

This Chapter summarizes the work carried out during the development of the thesis and comments on the results obtained.

Summary

- 5.1 Introduction
 - 5.2 Basic topology of a grid-connected three-phase three-wire inverter
 - 5.3 Deduction of the reference currents
 - 5.4 Voltage support concept
 - 5.5 Active and reactive power oscillations
 - 5.6 Analysis of the maximum injected current
 - 5.7 Analysis of the control algorithms
 - 5.8. Analysis of the voltage support capability
-

5.1 Introduction

This chapter shows in more detail the common thread of the whole research work, i.e., the argument of the present article-based thesis, in order to evidence how the manuscripts address related issues. The basic topology of a grid-connected three-phase three-wire inverter is the starting point since this system is the crucial element of study throughout the entire investigation. Next, the equations that give rise to the expressions of the reference currents in the manuscripts are deduced. These expressions are compared using tables to identify the similarities and differences that prevail when they are particularized either based on the selection of certain control parameters or based on performance conditions established by the control objectives.

Considering the expressions of the reference currents collect the necessary information from the system so that the control objectives are met, it is possible to analyze the impact they generate in terms of voltage support and power quality. These aspects are also discussed globally.

As expected, the common theme addressed by this thesis is identified from the Introduction, is developed in each of the intermediate chapters with a particular focus, and is globally discussed in this chapter in light of the information contained in the three manuscripts. As can be inferred, this approach offers the opportunity to explore the broader implications of the work.

5.2 Basic topology of a grid-connected three-phase three-wire inverter

Figure 5.1 shows a simplified, representative diagram of a three-phase three-wire voltage-sourced inverter (VSI) connected to an RL grid. It should be noted that the inverter is set in the power-controlled current source mode. An external controller provides the reference of generated active power (P_G) that should be injected into the grid. A dc-link

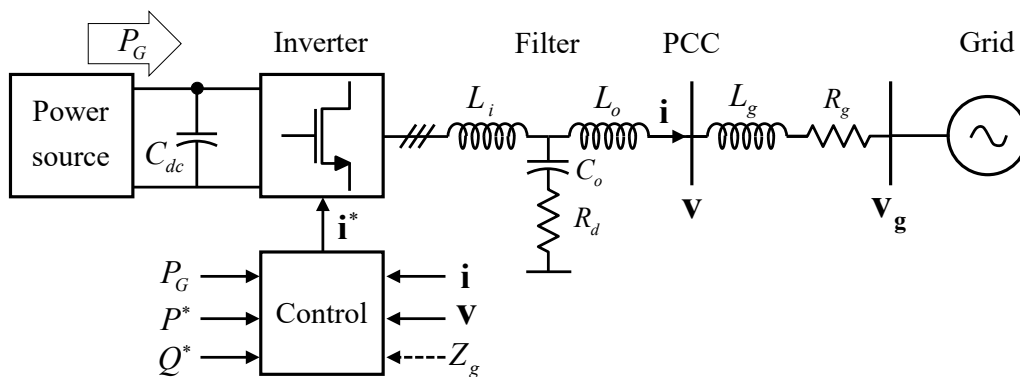


Figure 5.1. Simplified diagram of a grid-connected three-phase inverter.

capacitor C_{dc} operates the interconnection between the power source and the inverter to balance the power flow. The control block is responsible for driving the inverter switches in order to deliver power to the grid. The diagram also depicts a damped LCL filter, which is used to obtain a grid-side current with low harmonic content [85]. The inverter is connected to the grid at the point of common coupling (PCC), where the current and voltage vectors (\mathbf{i}, \mathbf{v}) are sensed. The grid is modeled as a voltage source \mathbf{v}_g and an equivalent grid impedance $Z_g = R_g + j\omega L_g$.

The configuration of the control loops allows the inverter to behave as a current source that is able to inject into the network a reference current \mathbf{i}^* demanded to support the power system. Mathematically, the reference current will have a general expression of the form $\mathbf{i}^* = f(P^*, Q^*, \mathbf{v})$, where P^* and Q^* are the references of active and reactive powers, respectively, and \mathbf{v} is the sensed voltage.

5.3 Deduction of the reference currents

As already explained above, it is possible to transform the instantaneous three-phase voltages at the PCC from the natural (abc) frame to the stationary $(\alpha\beta)$ frame by using Clarke's transformation

$$\begin{bmatrix} v_\alpha \\ v_\beta \end{bmatrix} = \frac{2}{3} \begin{bmatrix} 1 & -\frac{1}{2} & -\frac{1}{2} \\ 0 & \frac{\sqrt{3}}{2} & -\frac{\sqrt{3}}{2} \end{bmatrix} \begin{bmatrix} v_a \\ v_b \\ v_c \end{bmatrix} \quad (5.1)$$

where v_α and v_β , during voltage disturbances, can be expressed as the addition of their positive- and negative-symmetric sequences [86], [87]

$$v_\alpha = v_\alpha^+ + v_\alpha^- \quad (5.2)$$

$$v_\beta = v_\beta^+ + v_\beta^- \quad (5.3)$$

Therefore, based on the method of symmetrical components, positive- and negative-sequence voltages can be written as

$$v_\alpha^+ = V^+ \cos(\omega t + \phi^+) \quad (5.4)$$

$$v_\alpha^- = V^- \cos(\omega t + \phi^-) \quad (5.5)$$

$$v_\beta^+ = V^+ \sin(\omega t + \phi^+) \quad (5.6)$$

$$v_\beta^- = -V^- \sin(\omega t + \phi^-). \quad (5.7)$$

The difference of the initial phases (ϕ^+ and ϕ^-) is called the phase angle ϕ . This phase-angle difference is also formed between V^+ and V^- . The complete solution to determine the angle ϕ is obtained as [10]

$$\cos \phi = \frac{v_\alpha^+ v_\alpha^- - v_\beta^+ v_\beta^-}{V^+ V^-} \quad (5.8)$$

$$\sin \phi = \frac{v_\alpha^+ v_\beta^- + v_\beta^+ v_\alpha^-}{V^+ V^-} \quad (5.9)$$

$$\phi = \text{atan2}(\sin \phi, \cos \phi) \quad (5.10)$$

where atan2 is the two-argument arctangent function.

For the present analysis, the voltage unbalance factor (VUF), defined as the ratio of the V^- to the V^+ [88], will be identified by the letter u :

$$u = \frac{V^-}{V^+} = \frac{\sqrt{(v_\alpha^-)^2 + (v_\beta^-)^2}}{\sqrt{(v_\alpha^+)^2 + (v_\beta^+)^2}} \quad (5.11)$$

According to the power theory, the instantaneous active and reactive powers injected into the grid by a three-phase VSI can be expressed as

$$p = \frac{3}{2}(v_\alpha i_\alpha + v_\beta i_\beta) \quad (5.12)$$

$$q = \frac{3}{2}(v_\beta i_\alpha - v_\alpha i_\beta), \quad (5.13)$$

and using (5.12) and (5.13) it is possible to derive the expressions of the reference currents in the $\alpha\beta$ -frame:

$$i_\alpha^* = \frac{2}{3} \left(\frac{v_\alpha}{v_\alpha^2 + v_\beta^2} P^* + \frac{v_\beta}{v_\alpha^2 + v_\beta^2} Q^* \right) \quad (5.14)$$

$$i_\beta^* = \frac{2}{3} \left(\frac{v_\beta}{v_\alpha^2 + v_\beta^2} P^* - \frac{v_\alpha}{v_\alpha^2 + v_\beta^2} Q^* \right). \quad (5.15)$$

Now, using (5.2), (5.3), and (5.4)–(5.7) into (5.14) and (5.15), the denominator of these expressions can be developed to obtain

$$v_\alpha^2 + v_\beta^2 = (V^+)^2 + (V^-)^2 + V^+ V^- \cos(2\omega t + \phi^+ + \phi^-) \quad (5.16)$$

where an oscillating term at twice the fundamental grid frequency appears when unbalanced grid faults occur. This term produces harmonic distortion in the reference currents so it must disappear when low harmonic distortion is required. Therefore, the reference currents are expressed as

$$i_{\alpha}^* = \frac{2}{3} \left(\frac{v_{\alpha}^+ + v_{\alpha}^-}{(V^+)^2 + (V^-)^2} P^* + \frac{v_{\beta}^+ + v_{\beta}^-}{(V^+)^2 + (V^-)^2} Q^* \right) \quad (5.17)$$

$$i_{\beta}^* = \frac{2}{3} \left(\frac{v_{\beta}^+ + v_{\beta}^-}{(V^+)^2 + (V^-)^2} P^* - \frac{v_{\alpha}^+ + v_{\alpha}^-}{(V^+)^2 + (V^-)^2} Q^* \right). \quad (5.18)$$

The set of reference currents will include four control parameters (k_p^+ , k_p^- , k_q^+ , and k_q^-) to balance the positive- and negative-sequence voltages appropriately. Thus, the new set of flexible reference currents is defined as

$$i_{\alpha}^* = \frac{2}{3} \left(\frac{k_p^+ v_{\alpha}^+ + k_p^- v_{\alpha}^-}{k_p^+ (V^+)^2 + k_p^- (V^-)^2} P^* + \frac{k_q^+ v_{\beta}^+ + k_q^- v_{\beta}^-}{k_q^+ (V^+)^2 + k_q^- (V^-)^2} Q^* \right) \quad (5.19)$$

$$i_{\beta}^* = \frac{2}{3} \left(\frac{k_p^+ v_{\beta}^+ + k_p^- v_{\beta}^-}{k_p^+ (V^+)^2 + k_p^- (V^-)^2} P^* - \frac{k_q^+ v_{\alpha}^+ + k_q^- v_{\alpha}^-}{k_q^+ (V^+)^2 + k_q^- (V^-)^2} Q^* \right). \quad (5.20)$$

The control parameters can take different values within the range $[-1, 1]$, which gives rise to many injection possibilities. However, in this work, it is considered that the control parameters that balance the positive-sequence voltages are within the range $0 \leq k_{p,q}^+ \leq 1$, while the parameters that balance the negative-sequences voltages take their values in the range $-1 \leq k_{p,q}^- \leq 1$ [89].

Added to that, the amplitudes of the positive- and negative-sequence currents (I_p^+ , I_p^- , I_q^+ , and I_q^-) associated with the active and reactive powers (P^* and Q^*) can be identified from (5.19) and (5.20) as

$$I_p^+ = \frac{2}{3} \frac{k_p^+ V^+}{k_p^+ (V^+)^2 + k_p^- (V^-)^2} P^* \quad (5.21)$$

$$I_p^- = \frac{2}{3} \frac{k_p^- V^-}{k_p^+ (V^+)^2 + k_p^- (V^-)^2} P^* \quad (5.22)$$

$$I_q^+ = \frac{2}{3} \frac{k_q^+ V^+}{k_q^+ (V^+)^2 + k_q^- (V^-)^2} Q^* \quad (5.23)$$

$$I_q^- = \frac{2}{3} \frac{k_q^- V^-}{k_q^+ (V^+)^2 + k_q^- (V^-)^2} Q^*. \quad (5.24)$$

Therefore, (5.19) and (5.20) can be written in a general form as

$$i_{\alpha}^* = I_p^+ \left(\frac{v_{\alpha}^+}{V^+} \right) + I_p^- \left(\frac{v_{\alpha}^-}{V^-} \right) + I_q^+ \left(\frac{v_{\beta}^+}{V^+} \right) + I_q^- \left(\frac{v_{\beta}^-}{V^-} \right) \quad (5.25)$$

$$i_{\beta}^* = I_p^+ \left(\frac{v_{\beta}^+}{V^+} \right) + I_p^- \left(\frac{v_{\beta}^-}{V^-} \right) - I_q^+ \left(\frac{v_{\alpha}^+}{V^+} \right) - I_q^- \left(\frac{v_{\alpha}^-}{V^-} \right). \quad (5.26)$$

With this scheme, the reference currents follow both the positive- and negative-sequence voltages, which will reduce the voltage imbalance. If a control action is performed to increase V^+ , the voltage will be raised in all phases, and if V^- decreases, a voltage equalization is obtained [6].

Table 5.1 shows the schemes of the reference currents used in the publications that make up this thesis. The particularization of these schemes obeys the previous statement of a specific set of control objectives.

Table 5.1 Scheme of reference currents used in each journal article					
Journal	Reference currents	k_p^+	k_p^-	k_q^+	k_q^-
[1] (Ch. 2)	$i_{\alpha}^* = I_p^+ \left(\frac{v_{\alpha}^+}{V^+} \right) - I_p^- \left(\frac{v_{\alpha}^-}{V^-} \right) + I_q^+ \left(\frac{v_{\beta}^+}{V^+} \right) + I_q^- \left(\frac{v_{\beta}^-}{V^-} \right)$	1	-1	1	1
[2] (Ch. 3)	$i_{\beta}^* = I_p^+ \left(\frac{v_{\beta}^+}{V^+} \right) - I_p^- \left(\frac{v_{\beta}^-}{V^-} \right) - I_q^+ \left(\frac{v_{\alpha}^+}{V^+} \right) - I_q^- \left(\frac{v_{\alpha}^-}{V^-} \right)$				
[3] (Ch. 4)	$i_{\alpha}^* = I_p^+ \left(\frac{v_{\alpha}^+}{V^+} \right) + I_q^+ \left(\frac{v_{\beta}^+}{V^+} \right) + I_q^- \left(\frac{v_{\beta}^-}{V^-} \right)$ $i_{\beta}^* = I_p^+ \left(\frac{v_{\beta}^+}{V^+} \right) - I_q^+ \left(\frac{v_{\alpha}^+}{V^+} \right) - I_q^- \left(\frac{v_{\alpha}^-}{V^-} \right)$	1	0	1	1

5.4 Voltage support concept

It should be mentioned that the grid impedance must be known, for which different estimation techniques or methods can be used, including [90], [91]. From this perspective and based on Figure 5.1, the instantaneous voltages in the $a\beta$ channels at the PCC can be expressed as

$$v_{\alpha} = R_g i_{\alpha} + L_g \frac{di_{\alpha}}{dt} + v_{g\alpha} \quad (5.27)$$

$$v_{\beta} = R_g i_{\beta} + L_g \frac{di_{\beta}}{dt} + v_{g\beta} \quad (5.28)$$

where $v_{g\alpha}$ and $v_{g\beta}$ are the sag voltages at the grid side, R_g is the grid resistance, and L_g is the grid inductance. Then, the amplitudes of the positive- and negative-sequence voltages at the PCC side can be obtained using (5.25) and (5.26) in (5.27) and (5.28) as [34]

$$V^+ = R_g I_p^+ + \omega L_g I_q^+ + \sqrt{(V_g^+)^2 - (\omega L_g I_p^+ - R_g I_q^+)^2} \quad (5.29)$$

$$V^- = R_g I_p^- - \omega L_g I_q^- + \sqrt{(V_g^-)^2 - (\omega L_g I_p^- + R_g I_q^-)^2} . \quad (5.30)$$

Equations (5.29) and (5.30) can be rewritten and simplified as shown in the following:

$$V^+ \approx R_g I_p^+ + \omega L_g I_q^+ + V_g^+ \quad (5.31)$$

$$V^- \approx R_g I_p^- - \omega L_g I_q^- + V_g^- . \quad (5.32)$$

From (5.31) and (5.32), it can be said that voltage support is related to the different amplitudes of injected currents, but the optimal solution is closely linked to the equivalent grid impedance. Note that I_p^+ and I_q^+ act on V^+ and that I_p^- and I_q^- act on V^- . Likewise, by simple inspection, it can be deduced that if $k_p^+ = k_q^+ = k_q^- = 1$ and $k_p^- = -1$, then V^+ will increase and V^- will decrease when power is injected into the grid.

Table 5.2 summarizes the main combinations of these parameters according to different voltage support possibilities (control objectives) that could be achieved. The upwards arrow (\uparrow) means that this selection of parameters increases the value of the voltage amplitude (V^+ or V^-) it accompanies. The downwards arrow (\downarrow) represents the opposite. Also, the blue color denotes that the result is adequate or expected, while the red color indicates that this effect (or result) should be avoided.

Table 5.2					
Control parameters (k_p^+ , k_q^+ , k_p^- , and k_q^-)					
k_p^+	k_p^-	Objectives	k_q^+	k_q^-	Objectives
1	0	$\uparrow V^+$	1	0	$\uparrow V^+$
0	1	$\uparrow V^-$	0	1	$\downarrow V^-$
1	1	$\uparrow V^+$ and $\uparrow V^-$	1	1	$\uparrow V^+$ and $\downarrow V^-$ $\tilde{p} = 0$
1	-1	$\uparrow V^+$ and $\downarrow V^-$ $\tilde{p} = 0$	1	-1	$\tilde{q} = 0$ ($P^* = 0$)

As can be seen from Table 5.2, the shaded rows suggest that this selection of parameters is the most appropriate to increase V^+ and decrease V^- , at the same time as the oscillations in the active power are eliminated ($\tilde{p} = 0$).

5.5 Active and reactive power oscillations

To better understand the behavior of these control parameters in the cancellation of active power oscillations, it is necessary to decompose the instantaneous active and reactive powers—injected by the VSI—into their positive, negative, and oscillating components as [13]. Thus substituting (5.4)–(5.7), (5.19), and (5.20) into (5.12) and (5.13) yields:

$$\begin{aligned}
 p = & \frac{k_p^+(V^+)^2 + k_p^-(V^-)^2}{k_p^+(V^+)^2 + k_p^-(V^-)^2} P^* \\
 & + \frac{(k_p^+ + k_p^-)V^+V^- \cos(2\omega t + \phi^+ + \phi^-)}{k_p^+(V^+)^2 + k_p^-(V^-)^2} P^* \\
 & + \frac{(k_q^+ - k_q^-)V^+V^- \sin(2\omega t + \phi^+ + \phi^-)}{k_q^+(V^+)^2 + k_q^-(V^-)^2} Q^*
 \end{aligned} \tag{5.33}$$

$$\begin{aligned}
 q = & \frac{k_q^+(V^+)^2 + k_q^-(V^-)^2}{k_q^+(V^+)^2 + k_q^-(V^-)^2} Q^* \\
 & + \frac{(k_q^+ + k_q^-)V^+V^- \cos(2\omega t + \phi^+ + \phi^-)}{k_q^+(V^+)^2 + k_q^-(V^-)^2} Q^* \\
 & - \frac{(k_p^+ - k_p^-)V^+V^- \sin(2\omega t + \phi^+ + \phi^-)}{k_p^+(V^+)^2 + k_p^-(V^-)^2} P^*
 \end{aligned} \tag{5.34}$$

Equation (5.33) verifies that oscillations in the active power become zero in all cases exposed in [1] except in case 6 in which just positive-sequence reactive current (I_q^+) is injected due to severe grid fault conditions. The above is equivalent to saying that $k_p^+ = k_p^- = k_q^- = 0$ and $k_q^+ = 1$, in case 6, concerning Table 5.2. Avoiding active power oscillations is not a control objective in [3], and therefore no negative-sequence active current (I_p^-) is injected.

In order to avoid reactive power oscillations [see (5.34)], it would be necessary to select $k_p^+ = k_p^- = 1$, values that generate active power oscillations—which would not be convenient—or not to inject active power ($P^* = 0$). In any case, active power ripple will appear.

5.6 Analysis of the maximum injected current

Limiting the maximum output current of the inverter to a specific value has always been an essential control objective to guarantee its safe operation. Usually, this value corresponds to the nominal/rated current of the inverter (I_{rated}).

Assuming that the currents injected by the inverter into the grid follow their references, i.e., $i_\alpha \approx i_\alpha^*$ and $i_\beta \approx i_\beta^*$, the amplitudes of the phase currents can be calculated by replacing (5.4)–(5.7) into (5.19) and (5.20) and applying the inverse Clarke's transformation. Concerning these amplitudes, the phase currents on the abc reference frame can be expressed as a function of different variables such as the positive- and negative-sequence voltages (V^- and V^+) and the reference powers (P^* and Q^*), the positive- and negative-sequence active and reactive currents (I_p^+ , I_p^- , I_q^+ , and I_q^-), the positive- and negative-sequence currents (I^+ and I^-) calculated as (5.35) and (5.36), respectively, and the angle between positive and negative sequences (ϕ or ϕ_i).

$$I^+ = \sqrt{(I_p^+)^2 + (I_q^+)^2} \quad (5.35)$$

$$I^- = \sqrt{(I_p^-)^2 + (I_q^-)^2} \quad (5.36)$$

Journal	Maximum current
[1] (Ch. 2)	$I_{\max} = \sqrt{\frac{(V^+)^2 + (V^-)^2 - 2V^+V^-x}{(V^+)^2} \left((I_p^+)^2 + (I_q^+)^2 \right)}$
[2] (Ch. 3)	$I_{\max} = \frac{2}{3} \sqrt{\left((V^+)^2 + (V^-)^2 - 2V^+V^-x \right) z}$
[3] (Ch. 4)	$I_{\max} = \sqrt{(I_p^+)^2 + (I_q^+)^2 + (I_q^-)^2 + 2I_q^-I^+y}$

Table 5.3 shows the mathematical expressions used in each article of this thesis to calculate and, at the same time, limit the maximum current injected by the inverter into the grid, where

$$x = \min \left\{ \cos(\phi), \cos\left(\phi - \frac{2}{3}\pi\right), \cos\left(\phi + \frac{2}{3}\pi\right) \right\} \quad (5.37)$$

$$y = \max \left\{ \cos(\phi_i), \cos\left(\phi_i + \frac{2}{3}\pi\right), \cos\left(\phi_i - \frac{2}{3}\pi\right) \right\} \quad (5.38)$$

$$\phi_i = \text{atan2}(I_q^+, I_p^+) + \frac{\pi}{2} - \phi \quad (5.39)$$

$$z = \left(\frac{P^*}{(V^+)^2 - (V^-)^2} \right)^2 + \left(\frac{Q^*}{(V^+)^2 + (V^-)^2} \right)^2. \quad (5.40)$$

However, to be able to compare the expressions of the maximum current throughout this analysis, it is necessary to obtain a general equation from (5.25) and (5.26). Therefore, substituting (5.4)–(5.7) into (5.25) and (5.26) generates the following set of equations:

$$i_\alpha^* = I_p^+ \cos(\omega t + \phi^+) + I_p^- \cos(\omega t + \phi^-) + I_q^+ \sin(\omega t + \phi^+) - I_q^- \sin(\omega t + \phi^-) \quad (5.41)$$

$$i_\beta^* = I_p^+ \sin(\omega t + \phi^+) - I_p^- \sin(\omega t + \phi^-) - I_q^+ \cos(\omega t + \phi^+) - I_q^- \cos(\omega t + \phi^-). \quad (5.42)$$

Now, taking into account that $f_a(t) = f_\alpha(t)$ [92], the amplitude of I_a will be obtained from (5.41) to particularize the expression of the maximum current according to the control objectives proposed in each of the publications of this thesis. Then,

$$I_a = \sqrt{(I_p^+)^2 + (I_p^-)^2 + (I_q^+)^2 + (I_q^-)^2 + 2A \cos(\phi) + 2B \sin(\phi)} \quad (5.43)$$

where

$$A = I_p^+ I_p^- - I_q^+ I_q^- \quad (5.44)$$

$$B = I_q^+ I_p^- + I_p^+ I_q^-. \quad (5.45)$$

The other two amplitudes are also expressed in terms of the positive- and negative-sequence active and reactive currents and the angle ϕ :

$$I_b = \sqrt{(I_p^+)^2 + (I_p^-)^2 + (I_q^+)^2 + (I_q^-)^2 + 2A \cos(\phi - \frac{2}{3}\pi) + 2B \sin(\phi - \frac{2}{3}\pi)} \quad (5.46)$$

$$I_c = \sqrt{(I_p^+)^2 + (I_p^-)^2 + (I_q^+)^2 + (I_q^-)^2 + 2A \cos(\phi + \frac{2}{3}\pi) + 2B \sin(\phi + \frac{2}{3}\pi)} \quad (5.47)$$

Based on Table 5.2 and (5.43)–(5.45), Table 5.4 compares the particularized expressions to calculate the amplitude I_a according to the control objectives formulated in each publication. It should be noted that in [1], [2] the negative-sequence currents are related to the positive-sequence ones through the VUF, as shown in (5.48) and (5.49), which allows simplifying and writing this amplitude as stated in Table 5.4.

$$I_p^- = \frac{k_p^- V^-}{k_p^+ V^+} I_p^+ \quad (5.48)$$

$$I_q^- = \frac{k_q^- V^-}{k_q^+ V^+} I_q^+ \quad (5.49)$$

Table 5.4 Amplitude of the phase current I_a in each journal article	
Journal	Phase current I_a
[1] (Ch. 2)	$I_a = \sqrt{(I_p^+)^2 + (I_p^-)^2 + (I_q^+)^2 + (I_q^-)^2 - 2u(I^+)^2 \cos(\phi)}$
[2] (Ch. 3)	
[3] (Ch. 4)	$I_a = \sqrt{(I_p^+)^2 + (I_q^+)^2 + (I_q^-)^2 + 2I_q^- (I_p^+ \sin(\phi) - I_q^+ \cos(\phi))}$

In order to identify the phase with the highest amplitude, it is important to analyze not only the sine and cosine functions but also the values and signs of the control parameters k_p^+ , k_p^- , k_q^+ , and k_q^- .

In this context, each case proposed in [1] is verified in order to demonstrate that equations (5.43)–(5.47) are a valid solution for any configuration of power injection:

- 1) Case 1: Normal operation and low P_G . Injection of positive- and negative-sequence active power during a voltage imbalance.
- 2) Case 2: Normal operation and high P_G . Injection of positive- and negative-sequence active power during a voltage imbalance.
- 3) Case 3: Moderate grid fault conditions and low P_G . Injection of positive- and negative-sequence active and reactive powers.
- 4) Case 4: Moderate grid fault conditions and medium P_G . Injection of positive- and negative-sequence active and reactive powers.
- 5) Case 5: Severe grid fault conditions. Injection of positive- and negative-sequence reactive power.
- 6) Case 6: Severe grid fault conditions. Injection of positive-sequence reactive power.

Table 5.5 groups and summarizes a wide variety of cases that have been treated in different works, but partially. On the other hand, it could be said that in [3] two cases are considered when a voltage sag occurs:

- 1) Case 1: Grid fault conditions and low P_G . Injection of positive-sequence active power and positive- and negative-sequence reactive power.
- 2) Case 2: Grid fault conditions and high P_G . Injection of positive-sequence active and reactive powers.

As can be seen in Table 5.4, the solution to determine the expression of the maximum phase current when injecting I_q^- is not immediate, so it is convenient to express the term $2I_q^- (I_p^+ \sin(\phi) - I_q^+ \cos(\phi))$ as $2I_q^- I^+ y$. When only I_p^+ and I_q^+ are injected, the solution

Table 5.5 Maximum currents on the abc reference frame according to each case in [1]	
Injection cases	Maximum current I_{\max}
Case 1 Case 2	$I_{\max} = \sqrt{(I_p^+)^2 + (I_p^-)^2 - 2I_p^+ I_p^-} x$
Case 3 Case 4	$I_{\max} = \sqrt{(I_p^+)^2 + (I_p^-)^2 + (I_q^+)^2 + (I_q^-)^2 - 2u(I^+)^2} x$
Case 5	$I_{\max} = \sqrt{(I_q^+)^2 + (I_q^-)^2 - 2I_q^+ I_q^-} x$
Case 6	$I_{\max} = I_q^+$

is simple, and the controller will just have to guarantee that the GC is met and that I_p^+ does not exceed the value of $I_{p\max}^+$.

5.7 Analysis of the control algorithms

The control algorithm of each power injection strategy is designed according to the proposed control objectives and is fundamental to achieve them. Figure 5.2 contrasts an abbreviated version of the three control algorithms used to obtain the experimental results of the articles included in this thesis. Amplitudes of the positive- and negative-sequence currents are used to give coherence to the analysis that is carried out in this chapter.

As stated at the top of each algorithm, [1] and [3] give priority to the injection of reactive power (Q) into the network according to a specific GC. Therefore, whenever a voltage sag occurs, the control will guarantee a minimum of reactive power and the maximum output current of the inverter.

Despite the apparent similarities, there are several differences between these two algorithms, in principle both manage multiple objectives, operate under a GC, and limit the inverter output current to a predetermined maximum value. However, the algorithm in [1] is part of an open-loop controller with six identified cases, including two during normal operation, that allows eliminating oscillations in the active power since it can inject I_p^- . By contrast, the algorithm in [3] is part of a closed-loop controller and does not cancel the active power oscillations because it does not inject I_p^- .

Another significant difference lies in the way each controller determines the new value of I_q^+ when there is not enough P_G , i.e., when $I_p^+ < I_{p\max}^+$. In [1] the value of I_q^+ , and therefore that of I_q^- , is mathematically recalculated, while in [3] these values are

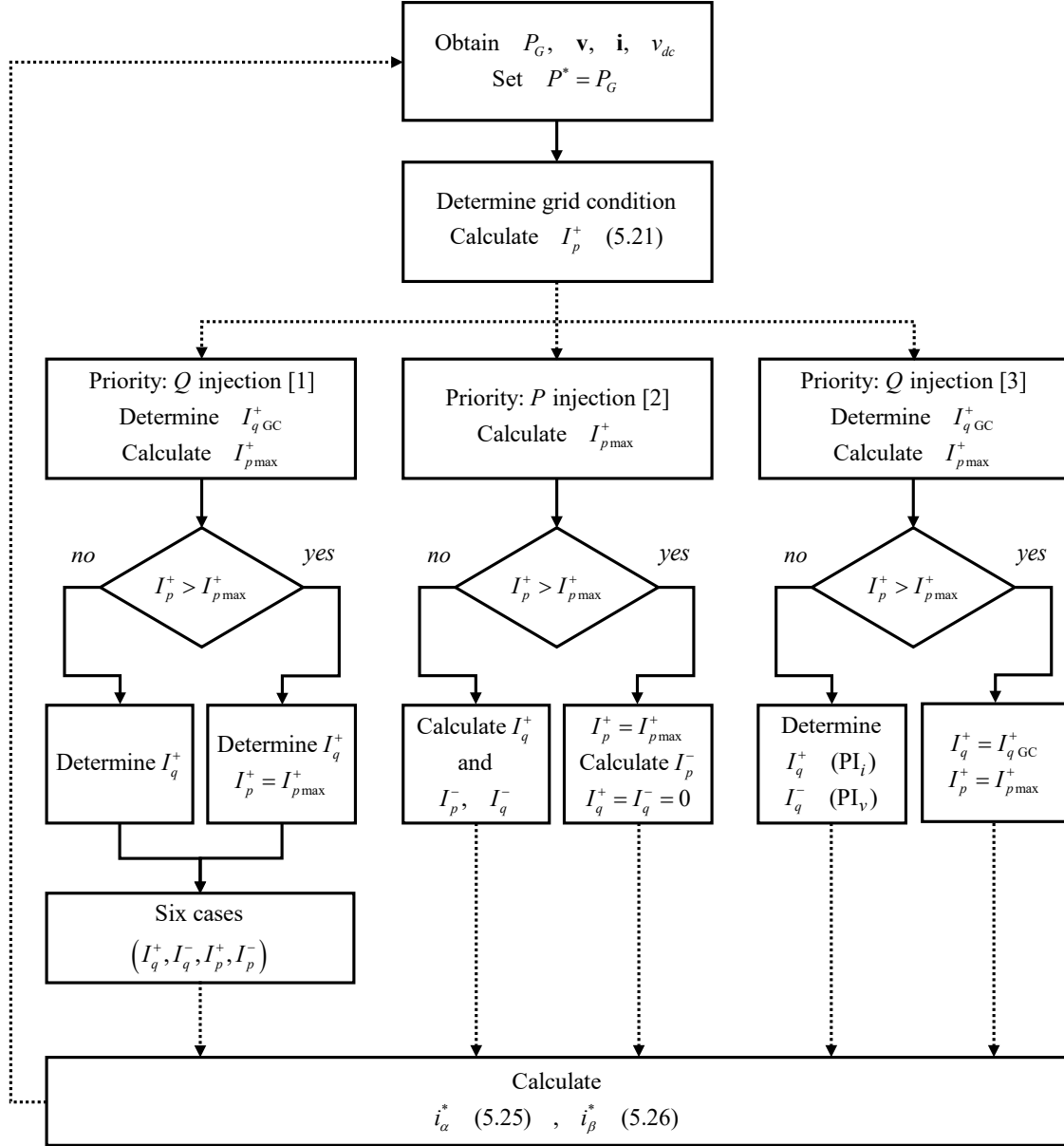


Figure 5.2. Comparison of the control algorithms.

determined by two PI controllers. It is worth mentioning that in [1] it was shown that I_{pmax}^+ could be zero, which would be equivalent to a total active power curtailment (APC).

The control algorithm cited in [2] is not a contribution of this research work, but it was used to perform all the experimental analysis about its effect on the voltage support when it is integrated into converters connected to RL networks. Note, as a first aspect, that it gives priority to the active power (P) delivery and that it will only deliver reactive power in P_G low-production scenarios under voltage sags, circumstances under which it will inject I_p^+, I_p^-, I_q^+ , and I_q^- . Secondly, it is also part of an open-loop controller capable of eliminating the oscillations of active power and limiting the output current of the inverter. Finally, when $I_p^+ < I_{pmax}^+$, the values of I_q^+ and I_q^- are also recalculated mathematically.

5.8 Analysis of the voltage support capability

The existing literature on control of grid-connected inverters is extensive and focuses particularly on mainly inductive networks. Most of these works are based on symmetrical components, a practical tool for understanding the operation of a three-phase system under unbalanced conditions [93]. For converters connected to mainly resistive networks, fewer works have been presented, but strategies for these systems can be derived from the first ones as evidenced in [30], a recent study in which a flexible voltage support strategy (VSS) in LV grids is proposed.

On the other hand, the grid impedance is not purely inductive nor is it strictly resistive in the case of LV networks. The line impedance consists of resistance, inductive reactance, and even capacitive reactance [35], [36]. Therefore, new control strategies for grid-connected inverters during voltage sags should include a safe scheme of power injection into the network, with voltage support capability, but depending on the grid impedance angle, as evidenced in the voltage support experimental analysis carried out in [2].

Nevertheless, works considering networks with complex impedance are also limited. Using this approach, a VSS that increases V^+ and injects I_{rated} is presented in [31]. A zero-sequence compensated VSS is proposed in [32]. The control strategy implemented in [33] maximizes the voltage in the lowest phase considering the impedance angle θ_g . Three different VSSs are introduced in [34], the first one maximizes V^+ , the second one minimizes V^- , and the last strategy maximizes the difference between V^+ and V^- . However, none of these strategies provides a global solution that performs optimal voltage support based on the grid impedance, eliminates the active power oscillations, and allows limiting the inverter output current to a specific value, all at the same time.

These considerations at least suggest that future updates of existing GCs should take into account aspects such as optimal voltage support, i.e., based on grid impedance, with control objectives that could be defined, for instance, as follows:

- 1) To maximize V^+ and minimize V^- :

$$\max \left\{ V^+ (I_p^+, I_q^+) - V^- (I_p^-, I_q^-) \right\}. \quad (5.50)$$

- 2) To regulate V^+ and V^- in order to avoid overvoltage:

$$\max \{V_a, V_b, V_c\} \leq 1.1 \text{ p.u.} \quad (5.51)$$

- 3) To limit the amount of injected current to the maximum allowed by the inverter:

$$\max \{I_a, I_b, I_c\} \leq I_{rated}. \quad (5.52)$$

- 4) To avoid oscillations in the instantaneous active power (p):

$$p = P + \tilde{p} = P^* + 0 = P^*. \quad (5.53)$$

This analysis will prove useful in expanding the understanding of how the proper computation of positive- and negative-sequence active and reactive currents is the key to achieving more complex, sophisticated control objectives in *RL* grids.

6

Conclusions and future work:

This Chapter concludes the present doctoral thesis and proposes some research guidelines for future works.

Summary

- 6.1 Conclusions of the thesis
 - 6.2 Future work
-

6.1 Conclusions of the thesis

This investigation set out to optimize the operation of grid-tied inverters, taking full advantage of their capabilities, since power-electronic converters have become a potent resource to support the new decentralized-renewable electric-power systems adequately. Hence, the following conclusions can be drawn from the present study:

- 1) The research results of this doctoral thesis represent a further step in the development of controllers in power grid environments with increasing penetration of distributed generation. The contributions of this work have explored the design of flexible controllers that allow improving the stability and quality of the network, ensuring safe and optimal use of available power in renewable energy sources connected to the utility grid.
- 2) The present study has offered a framework for the exploration of a broad and diverse set of cases that cover from the control of inverters under perturbed grid conditions—including voltage imbalances and voltage sags—following grid codes and injecting maximum output current, up to voltage regulation techniques in low power networks.
- 3) The research carried out in Chapter 2 is oriented to control of grid-connected inverters during voltage sags (including voltage imbalances) to meet grid codes and maximize power delivery. The control strategy improves network stability and ensures optimum use of entire power capability of inverters. This proposal can be incorporated in the new scenario of standardization allowing to satisfy a higher number of control objectives.
- 4) Chapter 3 has provided a theoretical and experimental study of a low-voltage ride-through strategy implemented into multiple inverters connected to the grid during voltage sags. The voltage support analysis for different generated-power profiles was carried out considering the real impedance (complex) of a functional network. The results have shown the importance of involving the grid impedance when designing or selecting a control strategy for distributed generation systems.
- 5) The inverter control structure presented in Chapter 4 also incorporates the use of grid codes, but now with the additional capability to regulate the voltage through a voltage control loop implemented to avoid overvoltage in non-faulty phases due to the reactive current injection. This controller is proposed for low-power rating distributed inverters where conventional voltage-support provided by large power plants is not available. Besides, the control system implementation requires a low computational burden because it is based on traditional PI control loops.

6.2 Future work

Several research lines derive from the development of this doctoral thesis, but the main challenges for future work would be the following:

- 1) The design of the control algorithm proposed in Chapter 2 makes up an interesting research line since it exposes a scheme that combines grid code specifications with multiple control objectives that interact with each other. Implementing new control algorithms in this context is an opportunity for further researches.
- 2) Research in control of multiple converters connected to the grid under voltage faults is a promising field of study, especially in RL networks in order to obtain optimal voltage support. The interest of the subject contrasts with the few works found in the literature and is a motivation to continue researching in this field.
- 3) Further research needs to examine more closely the links between voltage ride-through capability and optimal voltage support for three-phase three-wire inverters connected to RL grids during voltage sags. It would be interesting to develop new controllers that allow calculating reference currents according to the grid impedance angle and that, at the same time, guarantee both the safe operation of the inverter and the quality of power delivered into the network.
- 4) Another possible area of future research, for distributed generation inverters in RL grid-faulty networks, would be to investigate smart voltage-regulation strategies with robust controllers able to regulate the positive-sequence voltage to an appropriate value within the normal operation range, cancel the negative-sequence voltage, and suitably limit the maximum current injected by the inverter.

References

- [1] M. A. Garnica Lopez, J. L. Garcia de Vicuna, J. Miret, M. Castilla, and R. Guzman, "Control Strategy for Grid-Connected Three-Phase Inverters During Voltage Sags to Meet Grid Codes and to Maximize Power Delivery Capability," *IEEE Trans. Power Electron.*, vol. 33, no. 11, pp. 9360–9374, Nov. 2018.
- [2] M. Garnica, L. García de Vicuña, J. Miret, A. Camacho, and R. Guzmán, "Voltage Support Experimental Analysis of a Low-Voltage Ride-Through Strategy Applied to Grid-Connected Distributed Inverters," *Energies*, vol. 11, no. 8, p. 1949, Jul. 2018.
- [3] J. Miret, M. Garnica, M. Castilla, L. García de Vicuña, and A. Camacho, "PI-based controller for low-power distributed inverters to maximize reactive current injection while avoiding over voltage during voltage sags," *IET Power Electron.*
- [4] M. Castilla, J. Miret, J. L. Sosa, J. Matas, and L. G. de Vicuña, "Grid-Fault Control Scheme for Three-Phase Photovoltaic Inverters With Adjustable Power Quality Characteristics," *IEEE Trans. Power Electron.*, vol. 25, no. 12, pp. 2930–2940, Dec. 2010.
- [5] J. Miret, M. Castilla, A. Camacho, L. G. de Vicuña, and J. Matas, "Control Scheme for Photovoltaic Three-Phase Inverters to Minimize Peak Currents During Unbalanced Grid-Voltage Sags," *IEEE Trans. Power Electron.*, vol. 27, no. 10, pp. 4262–4271, Oct. 2012.
- [6] A. Camacho, M. Castilla, J. Miret, J. C. Vasquez, and E. Alarcon-Gallo, "Flexible Voltage Support Control for Three-Phase Distributed Generation Inverters Under Grid Fault," *IEEE Trans. Ind. Electron.*, vol. 60, no. 4, pp. 1429–1441, Apr. 2013.
- [7] J. Miret, A. Camacho, M. Castilla, L. G. de Vicuña, and J. Matas, "Control Scheme With Voltage Support Capability for Distributed Generation Inverters Under Voltage Sags," *IEEE Trans. Power Electron.*, vol. 28, no. 11, pp. 5252–5262, Nov. 2013.
- [8] M. Castilla, J. Miret, A. Camacho, J. Matas, and L. Garcia de Vicuna, "Voltage Support Control Strategies for Static Synchronous Compensators Under Unbalanced Voltage Sags," *IEEE Trans. Ind. Electron.*, vol. 61, no. 2, pp. 808–820, Feb. 2014.
- [9] M. Castilla, J. Miret, A. Camacho, L. Garcia de Vicuna, and J. Matas, "Modeling and Design of Voltage Support Control Schemes for Three-Phase Inverters Operating Under Unbalanced Grid Conditions," *IEEE Trans. Power Electron.*, vol. 29, no. 11, pp. 6139–6150, Nov. 2014.
- [10] A. Camacho, M. Castilla, J. Miret, R. Guzman, and A. Borrell, "Reactive Power Control for Distributed Generation Power Plants to Comply With Voltage Limits During Grid Faults," *IEEE Trans. Power Electron.*, vol. 29, no. 11, pp. 6224–6234, Nov. 2014.
- [11] A. Camacho, M. Castilla, J. Miret, A. Borrell, and L. G. de Vicuna, "Active and Reactive Power Strategies With Peak Current Limitation for Distributed Generation Inverters During Unbalanced Grid Faults," *IEEE Trans. Ind. Electron.*, vol. 62, no. 3, pp. 1515–1525, Mar. 2015.
- [12] J. Miret, A. Camacho, M. Castilla, J. L. García de Vicuña, and J. de la Hoz, "Reactive current injection protocol for low-power rating distributed generation sources under voltage sags," *IET Power Electron.*, vol. 8, no. 6, pp. 879–886, Jun. 2015.
- [13] J. L. Sosa, M. Castilla, J. Miret, J. Matas, and Y. A. Al-Turki, "Control Strategy to Maximize the Power Capability of PV Three-Phase Inverters During Voltage Sags," *IEEE Trans. Power Electron.*, vol. 31, no. 4, pp. 3314–3323, Apr. 2016.
- [14] S. Alepuz *et al.*, "Control Strategies Based on Symmetrical Components for Grid-Connected Converters Under Voltage Dips," *IEEE Trans. Ind. Electron.*, vol. 56, no. 6, pp. 2162–2173, Jun. 2009.

-
- [15] P. Rodriguez, G. Medeiros, A. Luna, M. C. Cavalcanti, and R. Teodorescu, "Safe current injection strategies for a STATCOM under asymmetrical grid faults," in *2010 IEEE Energy Conversion Congress and Exposition*, 2010, pp. 3929–3935.
- [16] F. Wang, J. L. Duarte, and M. A. M. Hendrix, "Pliant Active and Reactive Power Control for Grid-Interactive Converters Under Unbalanced Voltage Dips," *IEEE Trans. Power Electron.*, vol. 26, no. 5, pp. 1511–1521, May 2011.
- [17] P. Rodriguez, A. Luna, J. R. Hermoso, I. Etxeberria-Otadui, R. Teodorescu, and F. Blaabjerg, "Current control method for distributed generation power generation plants under grid fault conditions," in *IECON 2011 - 37th Annual Conference of the IEEE Industrial Electronics Society*, 2011, pp. 1262–1269.
- [18] C.-T. Lee, C.-W. Hsu, and P.-T. Cheng, "A Low-Voltage Ride-Through Technique for Grid-Connected Converters of Distributed Energy Resources," *IEEE Trans. Ind. Appl.*, vol. 47, no. 4, pp. 1821–1832, Jul. 2011.
- [19] J. A. Suul, A. Luna, P. Rodríguez, and T. Undeland, "Virtual-Flux-Based Voltage-Sensor-Less Power Control for Unbalanced Grid Conditions," *IEEE Trans. Power Electron.*, vol. 27, no. 9, pp. 4071–4087, Sep. 2012.
- [20] C. Tang, Y.-T. Chen, and Y. Chen, "PV Power System With Multi-Mode Operation and Low-Voltage Ride-Through Capability," *IEEE Trans. Ind. Electron.*, vol. 62, no. 12, pp. 7524–7533, Dec. 2015.
- [21] H.-C. Chen, C.-T. Lee, P.-T. Cheng, R. Teodorescu, and F. Blaabjerg, "A Low-Voltage Ride-Through Technique for Grid-connected Converters with Reduced Power Transistors Stress," *IEEE Trans. Power Electron.*, vol. 31, no. 12, pp. 8562–8571, 2016.
- [22] S. Mozumder, A. Dhar, S. S. Rangarajan, and S. P. Karthikeyan, "Coordinated operation of multiple inverter based renewable distributed generators as an active power injector and reactive power compensator," in *2014 International Conference on Computation of Power, Energy, Information and Communication (ICCPEIC)*, 2014, pp. 298–303.
- [23] Y.-D. Lee and S.-Y. Park, "Reactive power allocation control scheme for multiple grid connected inverters," in *2015 9th International Conference on Power Electronics and ECCE Asia (ICPE-ECCE Asia)*, 2015, pp. 2481–2488.
- [24] M. Velasco, P. Martí, J. Torres-Martínez, J. Miret, and M. Castilla, "On the optimal reactive power control for grid-connected photovoltaic distributed generation systems," in *IECON 2015 - 41st Annual Conference of the IEEE Industrial Electronics Society*, 2015, pp. 003755–003760.
- [25] A. Momeneh, M. Castilla, J. Miret, P. Martí, and M. Velasco, "Comparative study of reactive power control methods for photovoltaic inverters in low-voltage grids," *IET Renew. Power Gener.*, vol. 10, no. 3, pp. 310–318, Mar. 2016.
- [26] P. Martí, M. Velasco, J. Torres-Martínez, J. Miret, and M. Castilla, "Reactive power control for loss minimization in low-voltage distributed generation systems," in *2016 12th IEEE International Conference on Control and Automation (ICCA)*, 2016, pp. 371–376.
- [27] O. V. Kulkarni, S. Doolla, and B. G. Fernandes, "Mode Transition Control Strategy for Multiple Inverter-Based Distributed Generators Operating in Grid-Connected and Standalone Mode," *IEEE Trans. Ind. Appl.*, vol. 53, no. 6, pp. 5927–5939, Nov. 2017.
- [28] J. Miret, J. García de Vicuña, R. Guzmán, A. Camacho, and M. Moradi Ghahderijani, "A Flexible Experimental Laboratory for Distributed Generation Networks Based on Power Inverters," *Energies*, vol. 10, no. 10, p. 1589, Oct. 2017.
- [29] A. Camacho *et al.*, "Performance Comparison of Grid-Faulty Control Schemes for Inverter-Based Industrial Microgrids," *Energies*, vol. 10, no. 12, p. 2096, Dec. 2017.
- [30] X. Guo, X. Zhang, B. Wang, W. Wu, and J. M. Guerrero, "Asymmetrical Grid Fault Ride-Through Strategy of Three-Phase Grid-Connected Inverter Considering Network Impedance Impact in Low-Voltage Grid," *IEEE Trans. Power Electron.*, vol. 29, no. 3, pp. 1064–1068, Mar. 2014.

-
- [31] A. Camacho, M. Castilla, J. Miret, P. Marti, and M. Velasco, "Maximizing positive sequence voltage support in inductive-resistive grids for distributed generation inverters during voltage sags," in *IECON 2016 - 42nd Annual Conference of the IEEE Industrial Electronics Society*, 2016, pp. 2343–2348.
- [32] M. M. Shabestary and Y. A.-R. I. Mohamed, "Advanced Voltage Support and Active Power Flow Control in Grid-Connected Converters Under Unbalanced Conditions," *IEEE Trans. Power Electron.*, vol. 33, no. 2, pp. 1855–1864, Feb. 2018.
- [33] A. Camacho, M. Castilla, J. Miret, L. García de Vicuña, and M. A. Garnica López, "Control Strategy for Distribution Generation Inverters to Maximize the Voltage Support in the Lowest Phase During Voltage Sags," *IEEE Trans. Ind. Electron.*, vol. 65, no. 3, pp. 2346–2355, Mar. 2018.
- [34] A. Camacho, M. Castilla, J. Miret, L. G. de Vicuna, and R. Guzman, "Positive and Negative Sequence Control Strategies to Maximize the Voltage Support in Resistive–Inductive Grids During Grid Faults," *IEEE Trans. Power Electron.*, vol. 33, no. 6, pp. 5362–5373, Jun. 2018.
- [35] J. L. Blackburn and T. J. Domin, "Fundamental Units: Per Unit and Percent Values," in *Protective Relaying: Principles and Applications*, 3rd ed., Boca Raton, FL, USA: CRC Press, 2006.
- [36] J. L. Blackburn and T. J. Domin, "Line Protection," in *Protective Relaying: Principles and Applications*, 3rd ed., Boca Raton, FL, USA: CRC Press, 2006.
- [37] Ö. Göksu, R. Teodorescu, C. L. Bak, F. Iov, and P. C. Kjøer, "Impact of wind power plant reactive current injection during asymmetrical grid faults," *IET Renew. Power Gener.*, vol. 7, no. 5, pp. 484–492, Sep. 2013.
- [38] Z. Dai, H. Lin, H. Yin, and Y. Qiu, "A novel method for voltage support control under unbalanced grid faults and grid harmonic voltage disturbances," *IET Power Electron.*, vol. 8, no. 8, pp. 1377–1385, Aug. 2015.
- [39] A. Milicua, G. Abad, and M. A. Rodriguez Vidal, "Online Reference Limitation Method of Shunt-Connected Converters to the Grid to Avoid Exceeding Voltage and Current Limits Under Unbalanced Operation—Part I: Theory," *IEEE Trans. Energy Convers.*, vol. 30, no. 3, pp. 852–863, Sep. 2015.
- [40] A. Milicua, G. Abad, and M. A. Rodriguez Vidal, "Online Reference Limitation Method of Shunt-Connected Converters to the Grid to Avoid Exceeding Voltage and Current Limits Under Unbalanced Operation—Part II: Validation," *IEEE Trans. Energy Convers.*, vol. 30, no. 3, pp. 864–873, Sep. 2015.
- [41] M. Mirhosseini, J. Pou, and V. G. Agelidis, "Individual Phase Current Control With the Capability to Avoid Overvoltage in Grid-Connected Photovoltaic Power Plants Under Unbalanced Voltage Sags," *IEEE Trans. Power Electron.*, vol. 30, no. 10, pp. 5346–5351, Oct. 2015.
- [42] T. Neumann, T. Wijnhoven, G. Deconinck, and I. Erlich, "Enhanced Dynamic Voltage Control of Type 4 Wind Turbines During Unbalanced Grid Faults," *IEEE Trans. Energy Convers.*, vol. 30, no. 4, pp. 1650–1659, Dec. 2015.
- [43] F. Nejabatkhah, Y. Li, and B. Wu, "Control Strategies of Three-Phase Distributed Generation Inverters for Grid Unbalanced Voltage Compensation," *IEEE Trans. Power Electron.*, vol. 31, no. 7, pp. 5228–5241, 2016.
- [44] M. M. Shabestary and Y. A.-R. I. Mohamed, "Analytical Expressions for Multiobjective Optimization of Converter-Based DG Operation Under Unbalanced Grid Conditions," *IEEE Trans. Power Electron.*, vol. 32, no. 9, pp. 7284–7296, Sep. 2017.
- [45] F. Blaabjerg, R. Teodorescu, M. Liserre, and A. V. Timbus, "Overview of Control and Grid Synchronization for Distributed Power Generation Systems," *IEEE Trans. Ind. Electron.*, vol. 53, no. 5, pp. 1398–1409, Oct. 2006.
- [46] R. Teodorescu, M. Liserre, and P. Rodríguez, "Grid Converter Control for WTS," in *Grid Converters for Photovoltaic and Wind Power Systems*, Chichester, UK: John Wiley & Sons, Ltd, 2010, pp. 205–236.

- [47] G. M. Masters, "The Electric Power Industry," in *Renewable and Efficient Electric Power Systems*, Hoboken, NJ, USA: John Wiley & Sons, Inc., 2005, pp. 107–168.
- [48] Fedit, "Smart Grids y la Evolución de la Red Eléctrica." pp. 1–82, 2011.
- [49] E. C. dos Santos and E. R. Cabral da Silva, "Introduction," in *Advanced Power Electronics Converters: PWM Converters Processing AC Voltages*, Hoboken, NJ, USA: John Wiley & Sons, Inc, 2014, pp. 01–09.
- [50] Endesa, "Generación distribuida | ENDESA EDUCA," 2014. [Online]. Available: http://www.endesaeduca.com/Endesa_educa/recursos-interactivos/smart-city/generacion-distribuida. [Accessed: 15-May-2016].
- [51] A. Yadav and L. Srivastava, "Optimal placement of distributed generation: An overview and key issues," in *2014 International Conference on Power Signals Control and Computations (EPSCICON)*, 2014, no. January, pp. 1–6.
- [52] J. Morales, "La Red Inteligente de Energía y Comunicaciones: Generalidades y Visión de Futuro," in *Guía de Redes Inteligentes de energía y comunicación*, 2011, pp. 11–41.
- [53] J. C. Sidlofsky, "Distributed Generation in the Ontario Regulatory Context," in *Distributed Generation and The Future of Ontario's Electricity Grid*, 2008.
- [54] H. B. Püttgen, P. R. MacGregor, and F. C. Lambert, "Distributed Generation: Semantic Hype or the Dawn of a New Era?," *IEEE Power Energy Mag.*, vol. 1, no. 1, pp. 22–29, Jan. 2003.
- [55] J. M. Casas Úbeda *et al.*, *Educación medioambiental*. Editorial Club Universitario, 2008.
- [56] International Electrotechnical Commission, "Reducing carbon dioxide emissions – 'decarbonization,'" in *Coping with the Energy Challenge. The IEC's role from 2010 to 2030 (White Paper)*, Geneva, Switzerland, 2010, p. 70.
- [57] F. Iov, R. Teodorescu, F. Blaabjerg, B. Andresen, J. Birk, and J. Miranda, "Grid Code Compliance of Grid-Side Converter in Wind Turbine Systems," in *37th IEEE Power Electronics Specialists Conference*, 2006, pp. 1–7.
- [58] M. Tsili and S. Papathanassiou, "A review of grid code technical requirements for wind farms," *IET Renew. Power Gener.*, vol. 3, no. 3, p. 308, 2009.
- [59] M. Altin, O. Goksu, R. Teodorescu, P. Rodriguez, B.-B. Jensen, and L. Helle, "Overview of recent grid codes for wind power integration," in *2010 12th International Conference on Optimization of Electrical and Electronic Equipment*, 2010, pp. 1152–1160.
- [60] G. Kabashi, K. Kadriu, A. Gashi, and V. Komoni, "Wind grid code requirements regarding connection and operation of wind turbine in Kosovo," in *7th Mediterranean Conference and Exhibition on Power Generation, Transmission, Distribution and Energy Conversion (MedPower 2010)*, 2010, no. November, pp. 192–192.
- [61] C. Feltes, S. Engelhardt, J. Kretschmann, J. Fortmann, and I. Erlich, "Dynamic performance evaluation of DFIG-based wind turbines regarding new German grid code requirements," in *IEEE PES General Meeting*, 2010, pp. 1–7.
- [62] M. Mohseni, M. A. S. Masoum, and S. Islam, "Emergency control of DFIG-based wind turbines to meet new European Grid Code requirements," in *ISGT 2011*, 2011, pp. 1–6.
- [63] M. Mohseni and S. M. Islam, "Transient Control of DFIG-Based Wind Power Plants in Compliance With the Australian Grid Code," *IEEE Trans. Power Electron.*, vol. 27, no. 6, pp. 2813–2824, Jun. 2012.
- [64] Y. Yang, P. Enjeti, F. Blaabjerg, and H. Wang, "Suggested grid code modifications to ensure wide-scale adoption of photovoltaic energy in distributed power generation systems," in *2013 IEEE Industry Applications Society Annual Meeting*, 2013, pp. 1–8.
- [65] Y. Bae, T.-K. Vu, and R.-Y. Kim, "Implemental Control Strategy for Grid Stabilization of Grid-Connected PV System Based on German Grid Code in Symmetrical Low-to-Medium Voltage Network," *IEEE Trans. Energy Convers.*, vol. 28, no. 3, pp. 619–631, Sep. 2013.

- [66] Y. Yang, P. Enjeti, F. Blaabjerg, and H. Wang, "Wide-Scale Adoption of Photovoltaic Energy: Grid Code Modifications Are Explored in the Distribution Grid," *IEEE Ind. Appl. Mag.*, vol. 21, no. 5, pp. 21–31, Sep. 2015.
- [67] "P.O. 12.3. Requisitos de respuesta frente a huecos de tensión de las instalaciones eólica," Red Eléctrica de España (REE), Madrid, España, 2006.
- [68] "Grid Code for high and extra high voltage," E.ON Netz GmbH, Bayreuth, Germany, 2006.
- [69] "Portaria n.º 596/2010. Regulamento da Rede de Transporte," A Entidade Reguladora dos Serviços Energéticos, Lisboa, Portugal, 2010.
- [70] "Portaria n.º 596/2010. Regulamento da Rede de Distribuição," A Entidade Reguladora dos Serviços Energéticos, Lisboa, Portugal, 2010.
- [71] "Network Code for Requirements for Grid Connection Applicable to all Generators," ENTSO-E, Brussels, Belgium, 2013.
- [72] "Distribution Code Approved by CER," Distribution System Operator ESB Networks Limited, Dublin, Ireland, 2016.
- [73] "Commission Regulation (EU) 2016/631. Establishing a network code on requirements for grid connection of generators," The European Commission, Brussels, Belgium, 2016.
- [74] *IEEE Recommended Practice for Monitoring Electric Power Quality*. IEEE Std 1159™-2009 (Revision of IEEE Std 1159-1995), 2009.
- [75] S. Chattopadhyay, M. Mitra, and S. Sengupta, *Electric Power Quality*. Dordrecht: Springer Netherlands, 2011.
- [76] *Electromagnetic compatibility (EMC) - Part 2-5: Environment - Description and classification of electromagnetic environments*, no. 61000-2-5 ed2. IEC TR 61000-2-5:2011 | IEC, 2011.
- [77] "Waveform Characteristics of Voltage Sags: Statistical Analysis. TR-112692," EPRI, Palo Alto, CA, 1999.
- [78] "Distribution System Power Quality Assessment: Phase II—Voltage Sag and Interruption Analysis. 1001678," EPRI, Palo Alto, CA, 2003.
- [79] *IEEE Guide for Voltage Sag Indices*. IEEE Std 1564™-2014, 2014.
- [80] *IEEE Trial-Use Recommended Practice for Voltage Sag and Short Interruption Ride-Through Testing for End-Use Electrical Equipment Rated Less than 1000 V*. IEEE Std 1668™-2014, 2014.
- [81] A. Yazdani and R. Iravani, "Electronic Power Conversion," in *Voltage-Sourced Converters in Power Systems*, Hoboken, NJ, USA: John Wiley & Sons, Inc., 2010, pp. 1–20.
- [82] *IEEE Application Guide for IEEE Std 1547™, IEEE Standard for Interconnecting Distributed Resources with Electric Power Systems*. IEEE Std 1547.2-2008, 2009.
- [83] R. Teodorescu, M. Liserre, and P. Rodríguez, "Grid Requirements for PV," in *Grid Converters for Photovoltaic and Wind Power Systems*, Chichester, UK: John Wiley & Sons, Ltd, 2010, pp. 31–42.
- [84] R. Teodorescu, M. Liserre, and P. Rodríguez, "Grid Requirements for WT Systems," in *Grid Converters for Photovoltaic and Wind Power Systems*, Chichester, UK: John Wiley & Sons, Ltd, 2010, pp. 145–167.
- [85] J. Liu, L. Zhou, X. Yu, B. Li, and C. Zheng, "Design and analysis of an LCL circuit-based three-phase grid-connected inverter," *IET Power Electron.*, vol. 10, no. 2, pp. 232–239, Feb. 2017.
- [86] C. L. Fortescue, "Method of Symmetrical Co-Ordinates Applied to the Solution of Polyphase Networks," *Trans. Am. Inst. Electr. Eng.*, vol. XXXVII, no. 2, pp. 1027–1140, Jul. 1918.
- [87] R. Teodorescu, M. Liserre, and P. Rodríguez, "Grid Synchronization in Three-Phase Power Converters," in *Grid Converters for Photovoltaic and Wind Power Systems*, Chichester, UK: John Wiley & Sons, Ltd, 2010, pp. 169–204.

- [88] *IEEE Recommended Practice for Electric Power Distribution for Industrial Plants*. IEEE Std 141™-1993 (R1999), 1994.
- [89] Y. L. Sosa Rodríguez, “Control de Convertidores Trifásicos durante Huecos de Tensión,” Treball Final de Màster, Departament d’Enginyeria Electrònica, Universitat Politècnica de Catalunya, Barcelona, España, 2016.
- [90] L. Asiminoaei, R. Teodorescu, F. Blaabjerg, and U. Borup, “Implementation and Test of an Online Embedded Grid Impedance Estimation Technique for PV Inverters,” *IEEE Trans. Ind. Electron.*, vol. 52, no. 4, pp. 1136–1144, Aug. 2005.
- [91] A. Vidal *et al.*, “A Method for Identification of the Equivalent Inductance and Resistance in the Plant Model of Current-Controlled Grid-Tied Converters,” *IEEE Trans. Power Electron.*, vol. 30, no. 12, pp. 7245–7261, Dec. 2015.
- [92] A. Yazdani and R. Iravani, “Space Phasors and Two-Dimensional Frames,” in *Voltage-Sourced Converters in Power Systems*, Hoboken, NJ, USA: John Wiley & Sons, Inc., 2010, pp. 69–114.
- [93] J. L. Blackburn and T. J. Domin, “Symmetrical Components: A Review,” in *Protective Relaying: Principles and Applications*, 3rd ed., Boca Raton, FL, USA: CRC Press, 2006.